Einstein's 1918 Legacy

Gravitational waves, what they will tell us and how we are doing in detecting them

Rainer Weiss, MIT

University of Vermont

April 27, 2005

LIGO Scientific Collaboration Member Institutions

University of Adelaide ACIGA
Australian National University ACIGA
Balearic Islands University
California State Dominquez Hills
Caltech CACR
Caltech LIGO
Caltech Experimental Gravitation CEGG
Caltech Theory CART
University of Cardiff GEO
Carleton College
Cornell University
Fermi National Laboratory
University of Florida @ Gainesville
Glasgow University GEO
NASA-Goddard Spaceflight Center
University of Hannover GEO
Hobart – Williams University
India-IUCAA
IAP Nizhny Novgorod
Iowa State University
Joint Institute of Laboratory Astrophysics
Salish Kootenai College

LIGO Livingston LIGOLA
LIGO Hanford LIGOWA
Loyola New Orleans
Louisiana State University
Louisiana Tech University
MIT LIGO
Max Planck (Garching) GEO
Max Planck (Potsdam) GEO
University of Michigan
Moscow State University
NAOJ - TAMA
Northwestern University
University of Oregon
Pennsylvania State University
Southeastern Louisiana University
Southern University
Stanford University
Syracuse University
University of Texas@Brownsville
Washington State University@ Pullman
University of Western Australia ACIGA
University of Wisconsin@Milwaukee

697

SITZUNGSBERICHTE 1916.
XXXIII.

DER

KÖNIGLICH PREUSSISCHEN

AKADEMIE DER WISSENSCHAFTEN.

688 Sitzung der physikalisch-mathematischen Klasse vom 22. Juni 1916

Näherungsweise Integration der Feldgleichungen der Gravitation.

Von A. Einstein.

$$\gamma'_{\mu\nu} = \alpha_{\mu\nu} f(x_1 + i x_4) = \alpha_{\mu\nu} f(x - t). \qquad (15)$$

Dabei sind die $\alpha_{\mu\nu}$ Konstante; f ist eine Funktion des Arguments $x - t$. Ist der betrachtete Raum frei von Materie, d. h. verschwinden die $T_{\mu\nu}$, so sind die Gleichungen (6) durch diesen Ansatz erfüllt. Die Gleichungen (4) liefern zwischen den $\alpha_{\mu\nu}$ die Beziehungen

$$\left.\begin{aligned} \alpha_{11} + i\alpha_{14} &= 0 \\ \alpha_{12} + i\alpha_{24} &= 0 \\ \alpha_{13} + i\alpha_{34} &= 0 \\ \alpha_{14} + i\alpha_{44} &= 0 \end{aligned}\right\}. \qquad (16)$$

Von den 10 Konstanten $\alpha_{\mu\nu}$ sind daher nur 6 frei wählbar. Wir können die allgemeinste Welle der betrachteten Art daher aus Wellen von folgenden 6 Typen superponieren

$$\left.\begin{aligned} &\text{a)}\ \alpha_{11} + i\alpha_{14} = 0 \quad \alpha_{14} + i\alpha_{44} = 0 \\ &\text{b)}\ \alpha_{12} + i\alpha_{24} = 0 \\ &\text{c)}\ \alpha_{13} + i\alpha_{34} = 0 \\ &\text{d)}\ \alpha_{22} \neq 0 \\ &\text{e)}\ \alpha_{23} \neq 0 \\ &\text{f)}\ \alpha_{33} \neq 0 \end{aligned}\right\}. \qquad (17)$$

$$\text{d)}\ \frac{1}{i} t_{22} = \frac{f'^2}{4\varkappa} \alpha_{22}^2 = \frac{1}{4\varkappa} \left(\frac{\partial \gamma'_{22}}{\partial t}\right)^2$$

$$\text{e)}\ \frac{1}{i} t_{23} = \frac{f'^2}{4\varkappa} \alpha_{23}^2 = \frac{1}{4\varkappa} \left(\frac{\partial \gamma'_{23}}{\partial t}\right)^2$$

$$\text{f)}\ \frac{1}{i} t_{33} = \frac{f'^2}{4\varkappa} \alpha_{33}^2 = \frac{1}{4\varkappa} \left(\frac{\partial \gamma'_{33}}{\partial t}\right)^2$$

Es ergibt sich also, daß nur die Wellen des letzten Typs Energie transportieren, und zwar ist der Energietransport einer beliebigen ebenen Welle gegeben durch

$$I_x = \frac{1}{i} t_{41} = \frac{1}{4\varkappa} \left[\left(\frac{\partial \gamma'_{22}}{\partial t}\right)^2 + 2\left(\frac{\partial \gamma'_{23}}{\partial t}\right)^2 + \left(\frac{\partial \gamma'_{33}}{\partial t}\right)^2\right]. \qquad (18)$$

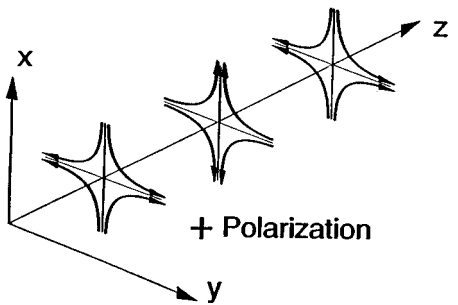
x
z
y
+ Polarization

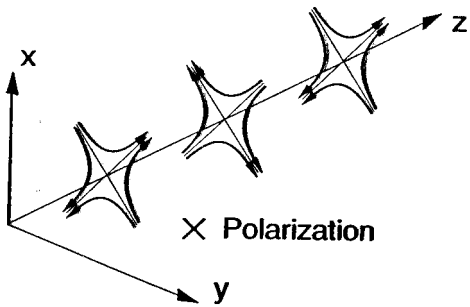
x
z
y
× Polarization

Die in (23), (23a) und (23b) auftretenden Integrale, welche nichts anderes sind als zeitlich variable Trägheitsmomente, nennen wir im folgenden zur Abkürzung J_{22}, J_{33}, J_{23}. Dann ergibt sich für die Intensität $\mathfrak{f}_x$ der Energiestrahlung aus (18)

$$\mathfrak{f}_x = \frac{\varkappa}{64\pi^2 R^2}\left[\left(\frac{\partial^3 J_{22}}{\partial t^3}\right)^2 + 2\left(\frac{\partial^3 J_{23}}{\partial t^3}\right)^2 + \left(\frac{\partial^3 J_{33}}{\partial t^3}\right)^2\right]. \qquad (20)$$

SPHERICALLY SYMMETRIC MOTION RADIATES GRAVITATIONAL WAVES

1918 VI. VII. VIII

SITZUNGSBERICHTE

DER

KÖNIGLICH PREUSSISCHEN

AKADEMIE DER WISSENSCHAFTEN

BERLIN 1918

VERLAG DER KÖNIGLICHEN AKADEMIE DER WISSENSCHAFTEN

IN KOMMISSION BEI GEORG REIMER

Über Gravitationswellen.

Von A. Einstein.

(Vorgelegt am 31. Januar 1918 [s. oben S. 79].)

Die wichtige Frage, wie die Ausbreitung der Gravitationsfelder erfolgt, ist schon vor anderthalb Jahren in einer Akademiearbeit von mir behandelt worden[1]. Da aber meine damalige Darstellung des Gegenstandes nicht genügend durchsichtig und außerdem durch einen bedauerlichen Rechenfehler verunstaltet ist, muß ich hier nochmals auf die Angelegenheit zurückkommen.

Wie damals beschränke ich mich auch hier auf den Fall, daß das betrachtete zeiträumliche Kontinuum sich von einem »galileischen« nur sehr wenig unterscheidet. Um für alle Indizes

$$g_{\mu\nu} = -\delta_{\mu\nu} + \gamma_{\mu\nu} \qquad (1)$$

Sind die Bedingungen (15) erfüllt, so stellt (14) eine mögliche Gravitationswelle dar. Um deren physikalische Natur genauer zu durchschauen, berechnen wir deren Dichte des Energiestromes $\frac{t_{41}}{i}$. Durch Einsetzen der in (15) gegebenen $\gamma'_{\mu\nu}$ in Gleichung (9) erhält man

$$\frac{t_{41}}{i} = \frac{1}{4\varkappa} f'^2 \left[\left(\frac{\alpha_{22} - \alpha_{33}}{2} \right)^2 + \alpha_{23}^2 \right]. \qquad (16)$$

$$\mathfrak{J}_{\mu\nu} = \int x_\mu x_\nu \rho \, dV_0 \tag{23}$$

gesetzt; $\mathfrak{J}_{\mu\nu}$ sind die Komponenten des (zeitlich variabeln) Trägheitsmomentes des materiellen Systems.

Auf analogem Wege erhält man

$$\int (T_{22} - T_{33}) \, dV_0 = \frac{1}{2} (\ddot{\mathfrak{J}}_{22} - \ddot{\mathfrak{J}}_{33}). \tag{24}$$

Aus (7a) ergibt sich auf Grund von (22) und (24)

$$\gamma'_{23} = - \frac{\varkappa}{4\pi R} \ddot{\mathfrak{J}}_{23}. \tag{25}$$

$$\frac{\gamma'_{22} - \gamma'_{33}}{2} = - \frac{\varkappa}{4\pi R} \left(\frac{\ddot{\mathfrak{J}}_{22} - \ddot{\mathfrak{J}}_{33}}{2} \right). \tag{26}$$

Die $\mathfrak{J}_{\mu\nu}$ sind nach (7a), (22), (24) für die Zeit $t - R$ zu nehmen, also Funktionen von $t - R$, oder bei großem R in der Nähe der x-Achse auch Funktionen von $t - x$. (25), (26) stellen also Gravitationswellen dar, deren Energiefluß längs der x-Achse gemäß (16) die Dichte

$$\frac{t_{41}}{i} = \frac{\varkappa}{64\pi^2 R^2} \left[\left(\frac{\dddot{\mathfrak{J}}_{22} - \dddot{\mathfrak{J}}_{33}}{2} \right)^2 + \dddot{\mathfrak{J}}_{23}^{\,2} \right] \tag{27}$$

besitzt.

Neutron Binary System – Hulse & Taylor

PSR 1913 + 16 -- Timing of pulsars

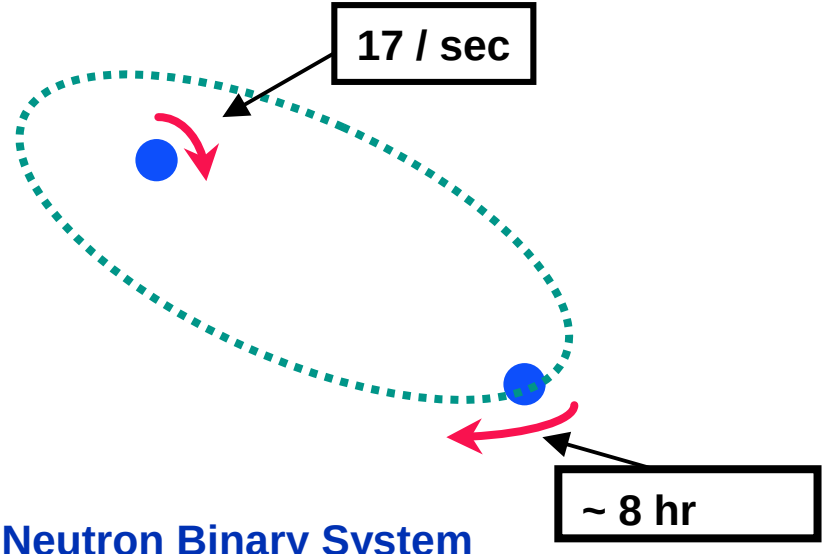

Neutron Binary System

- separated by 10^6 miles
- $m_1 = 1.4m_\odot$; $m_2 = 1.36m_\odot$; $\varepsilon = 0.617$

Prediction from general relativity

- spiral in by 3 mm/orbit
- rate of change orbital period

Emission of gravitational waves

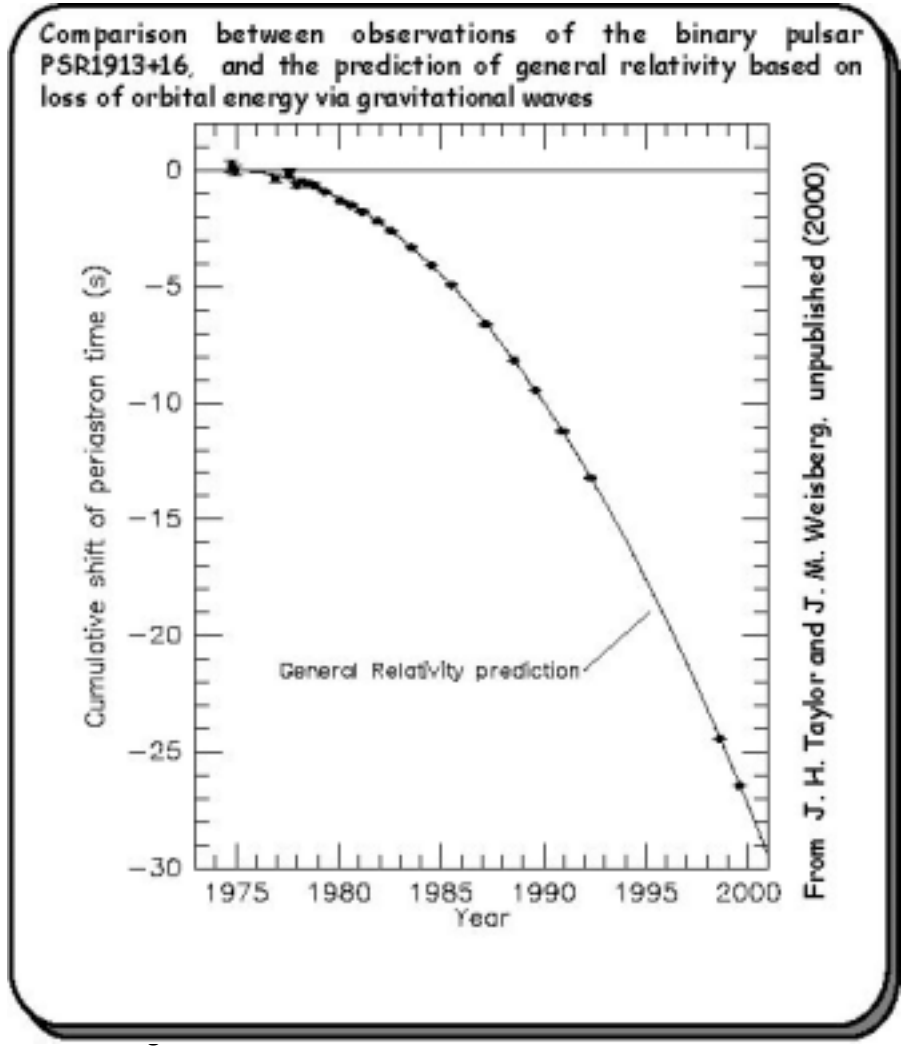

Direct detection of gravitational waves from astrophysical sources

- Physics
  - Observations of gravitation in the strong field, high velocity limit
  - Determination of wave kinematics – polarization and propagation
  - Tests for alternative relativistic gravitational theories
- Astrophysics
  - Measurement of coherent inner dynamics – stellar collapse, pulsar formation….
  - Compact binary coalescence – neutron star/neutron star, black hole/black hole
  - Neutron star equation of state
  - Primeval cosmic spectrum of gravitational waves
- Gravitational wave survey of the universe

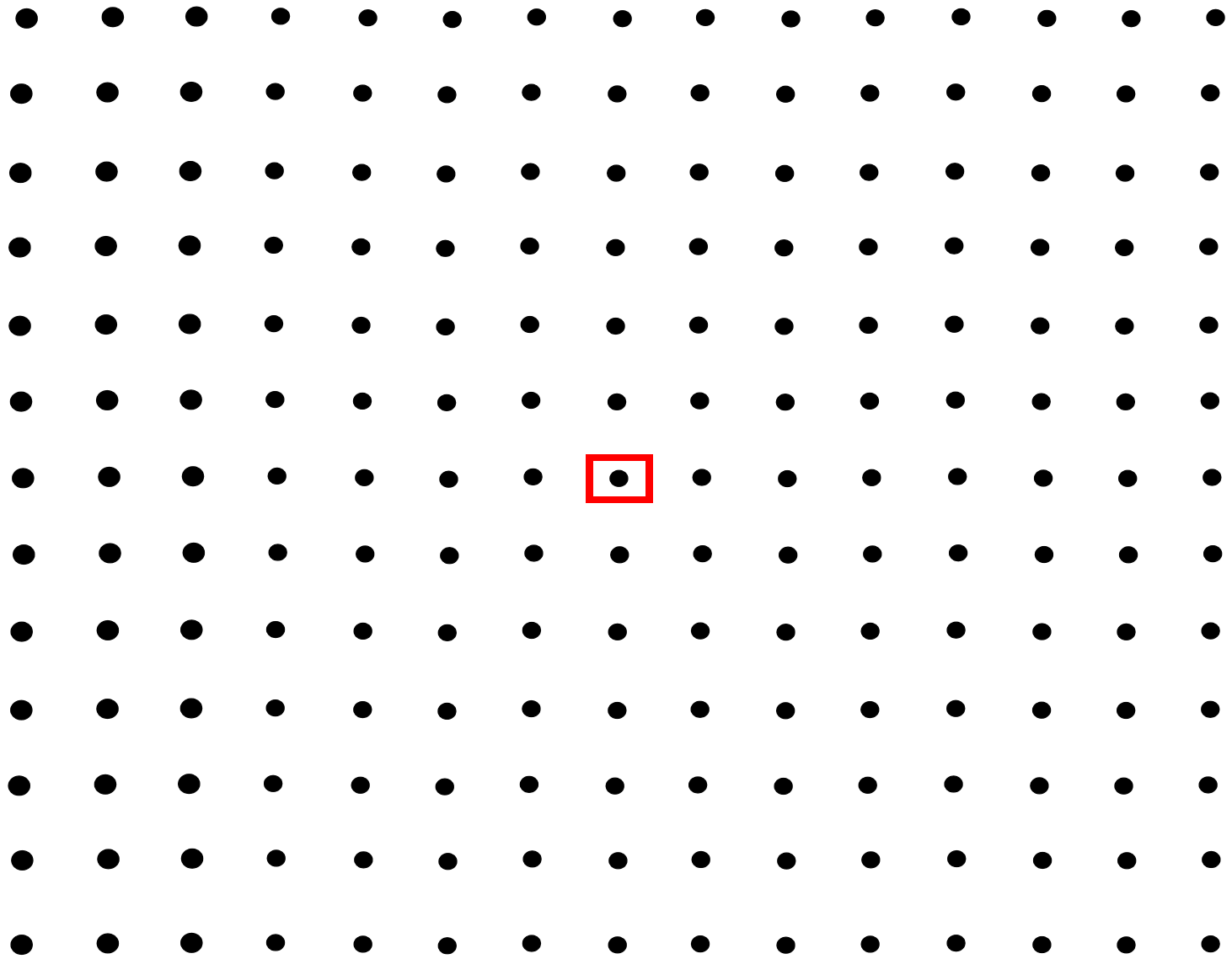

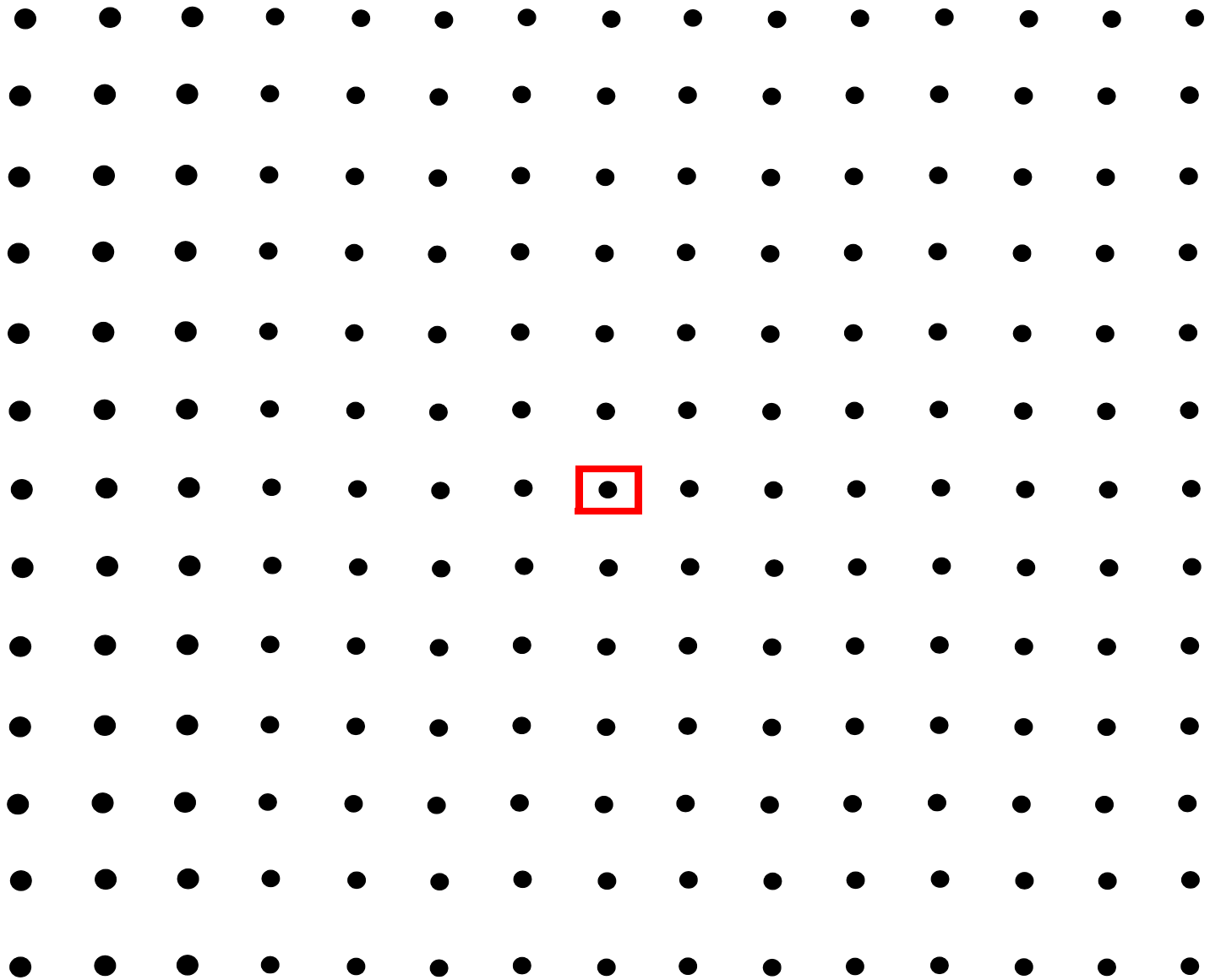

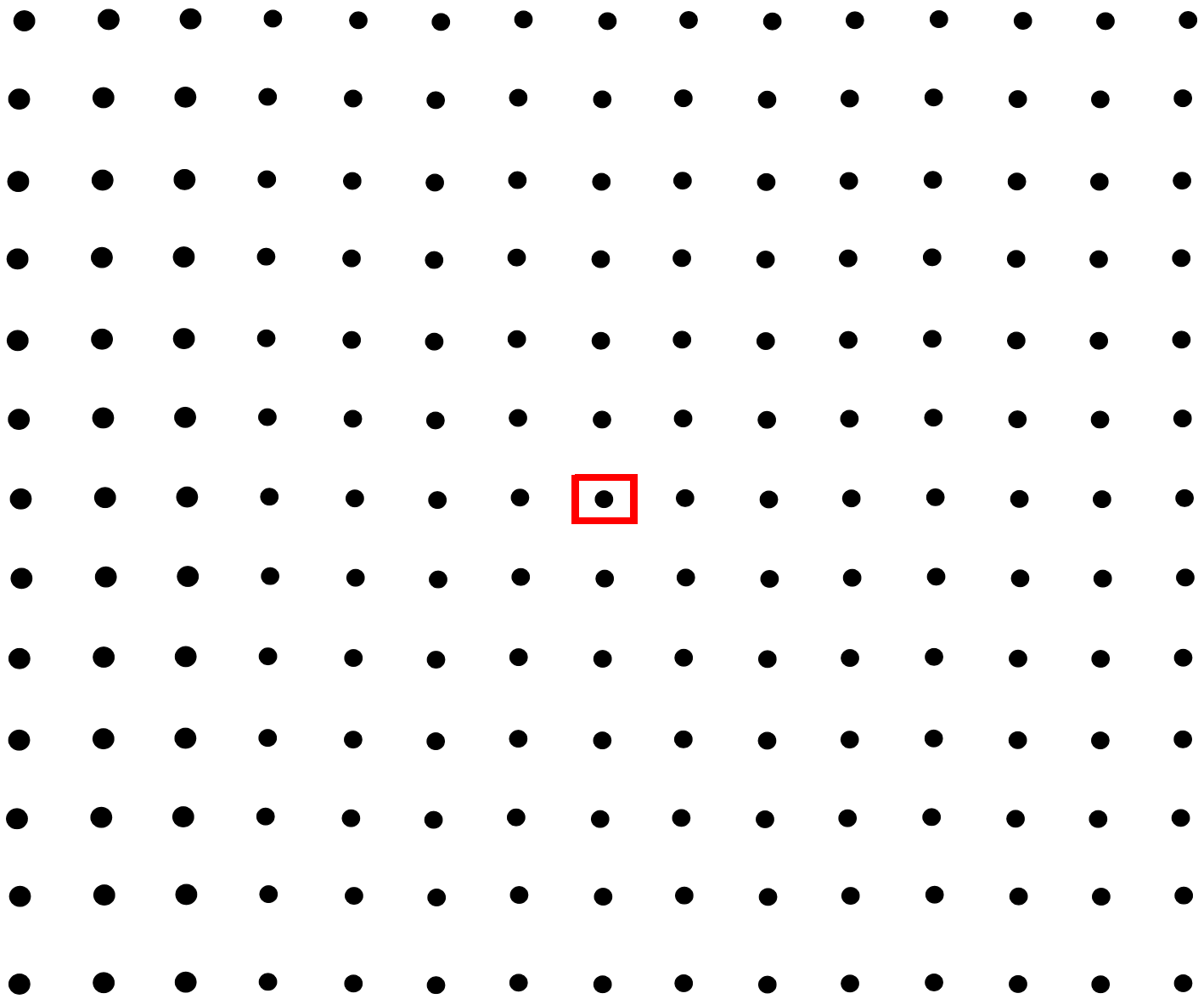

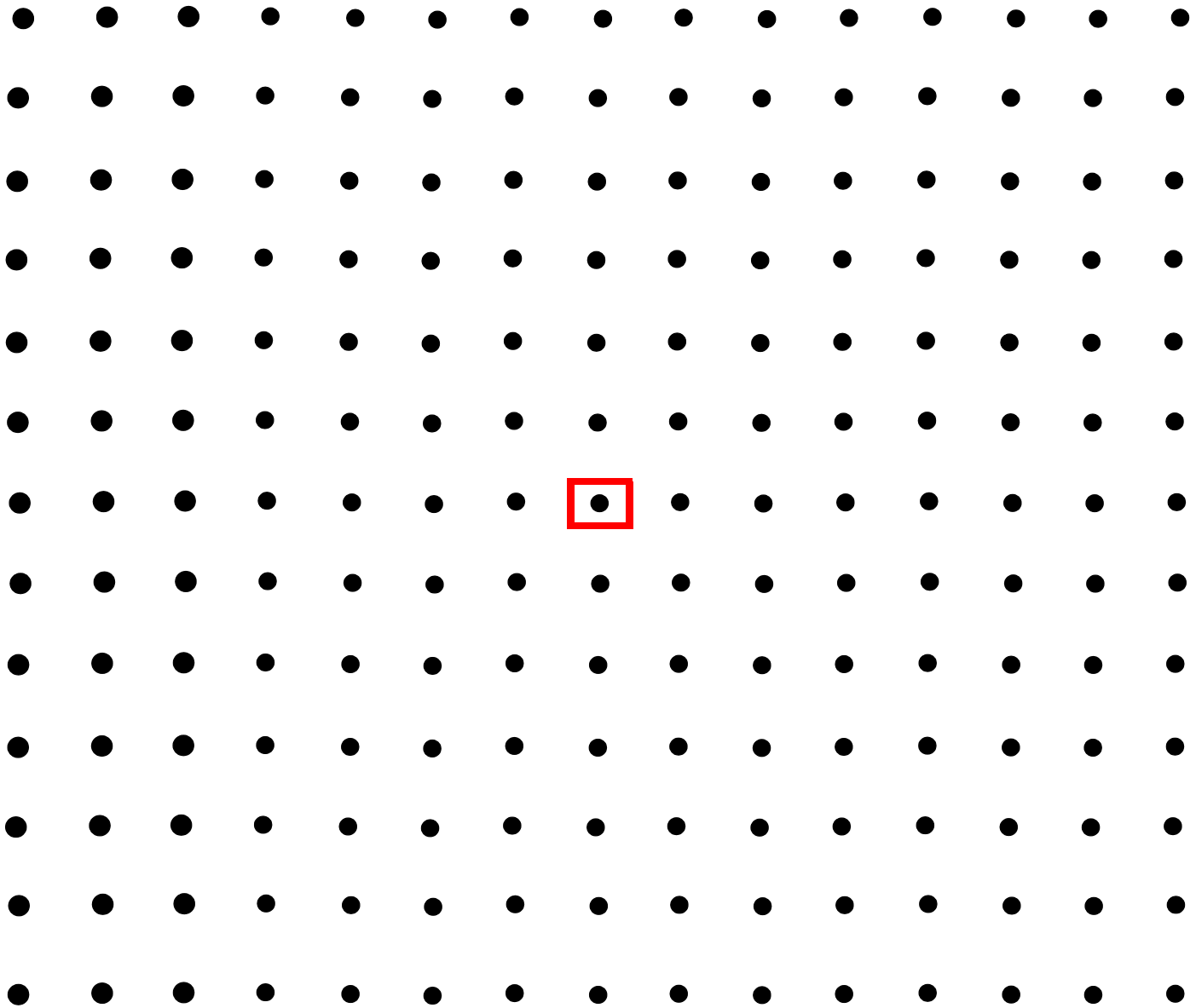

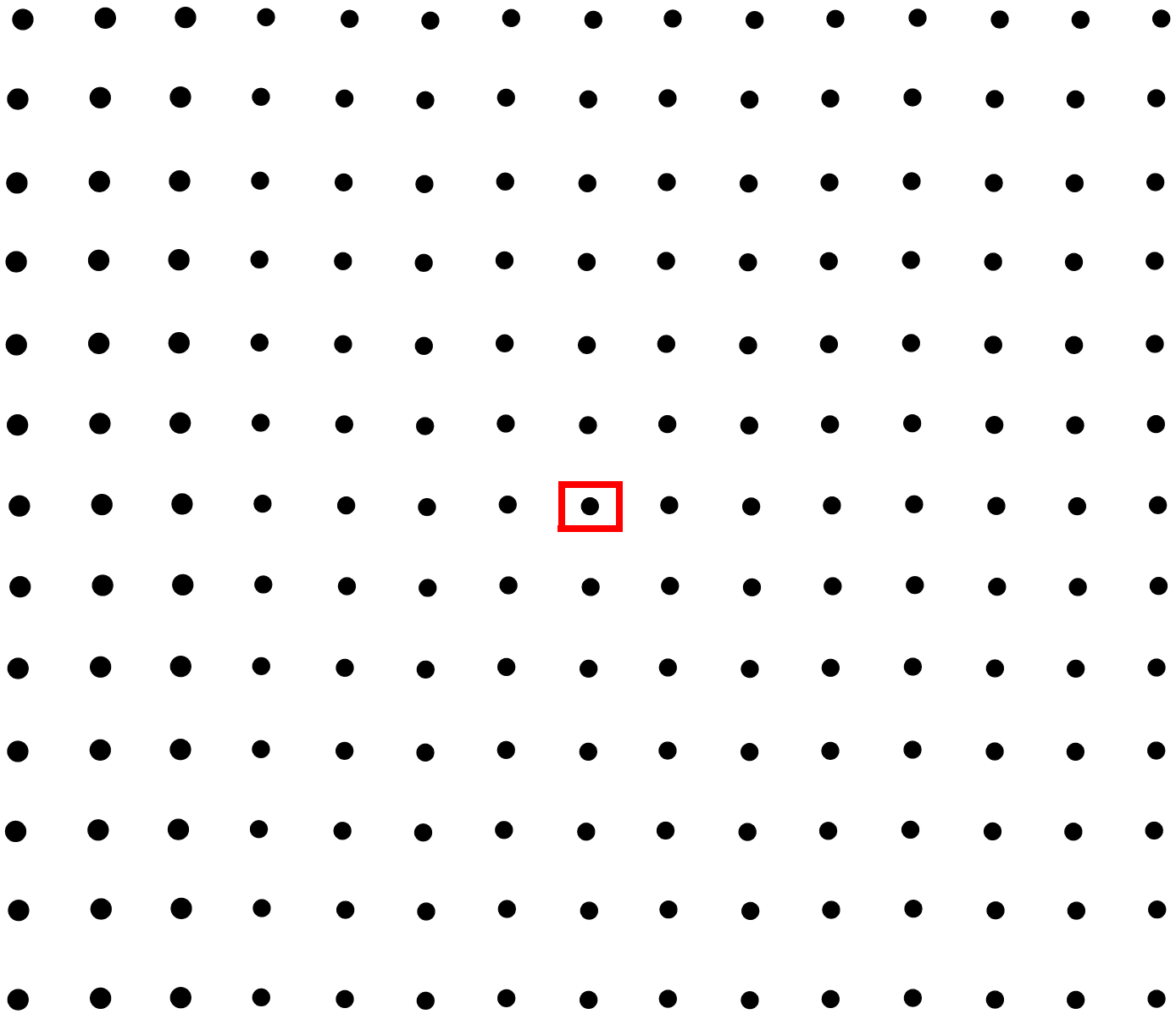

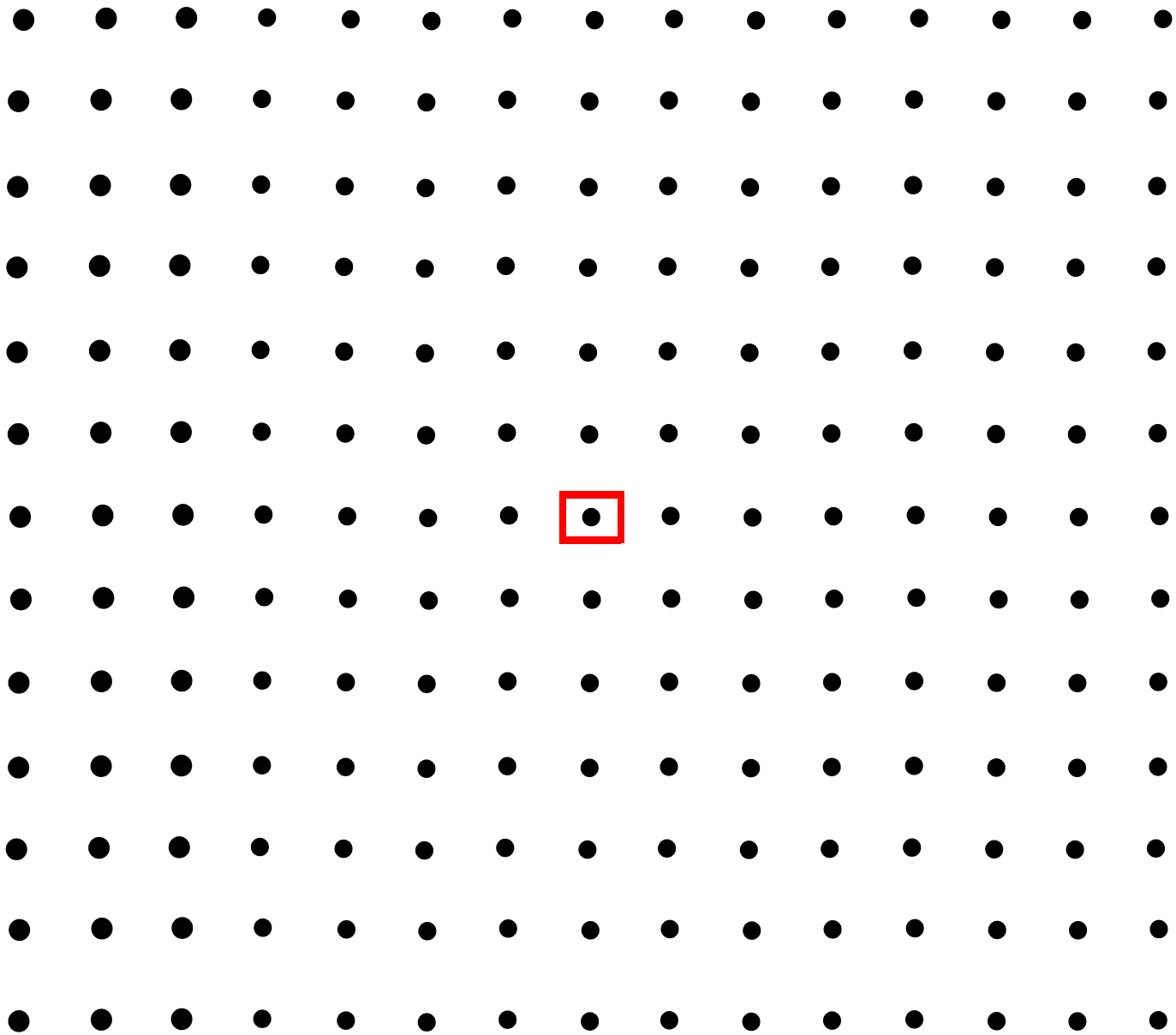

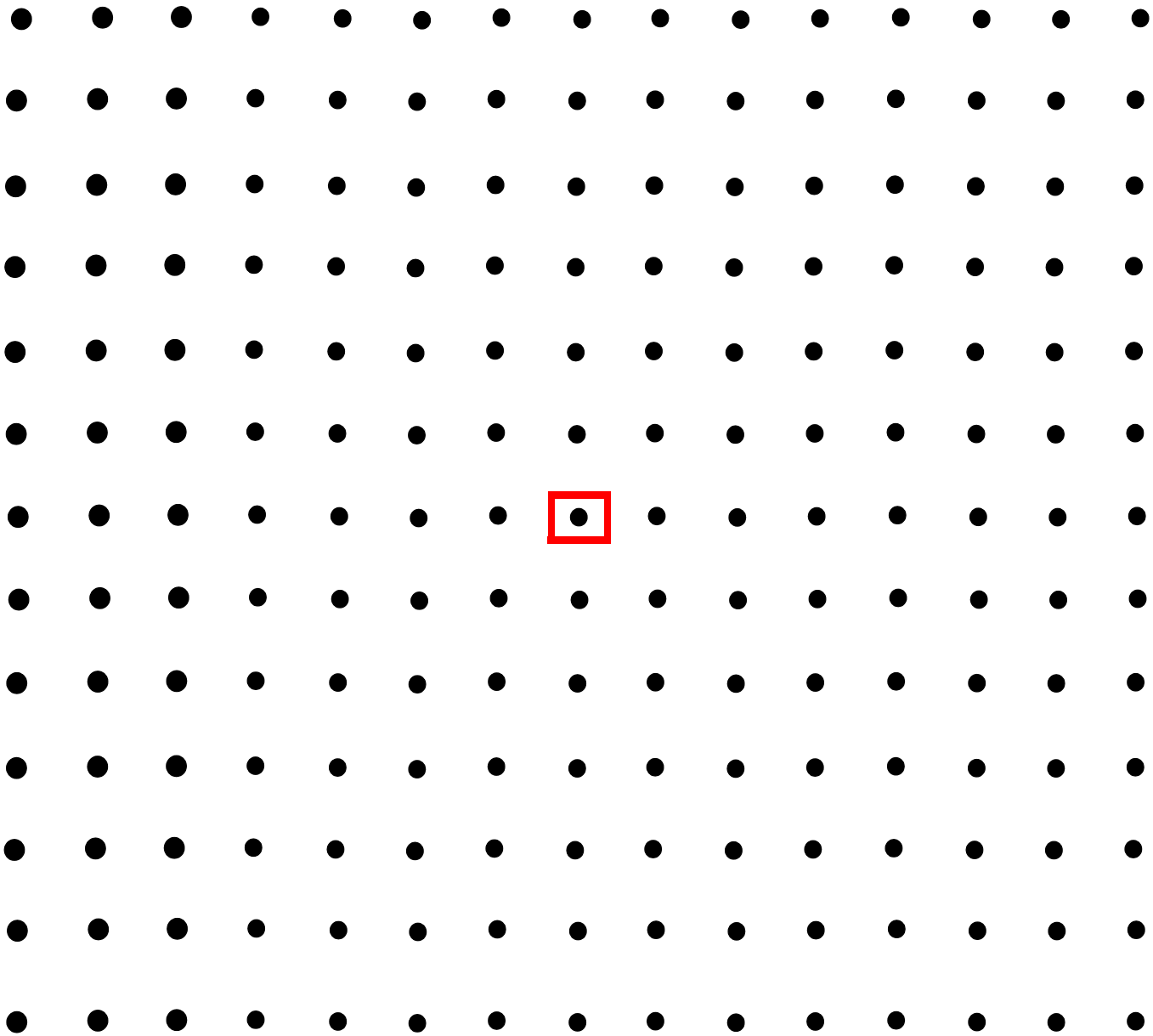

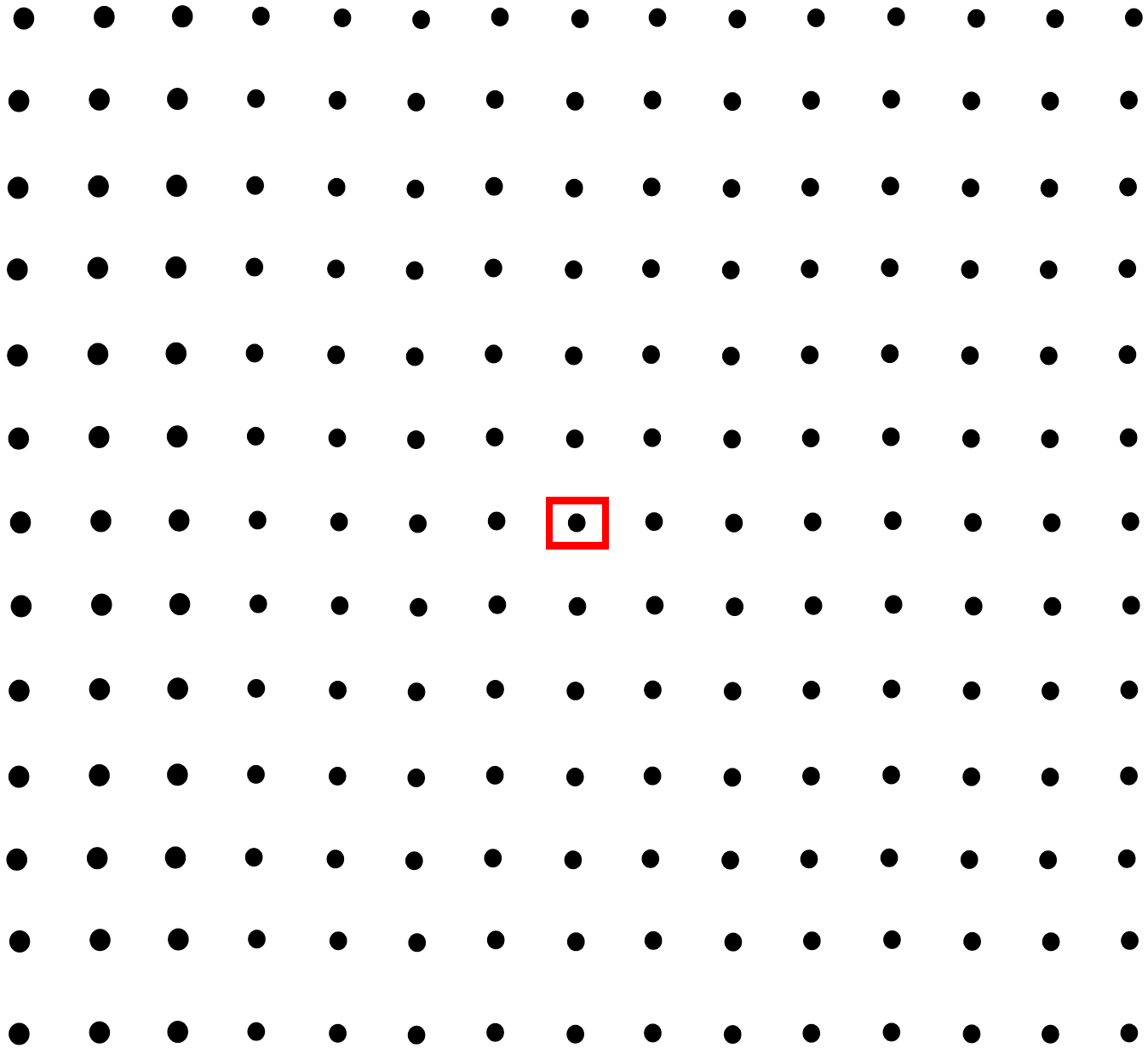

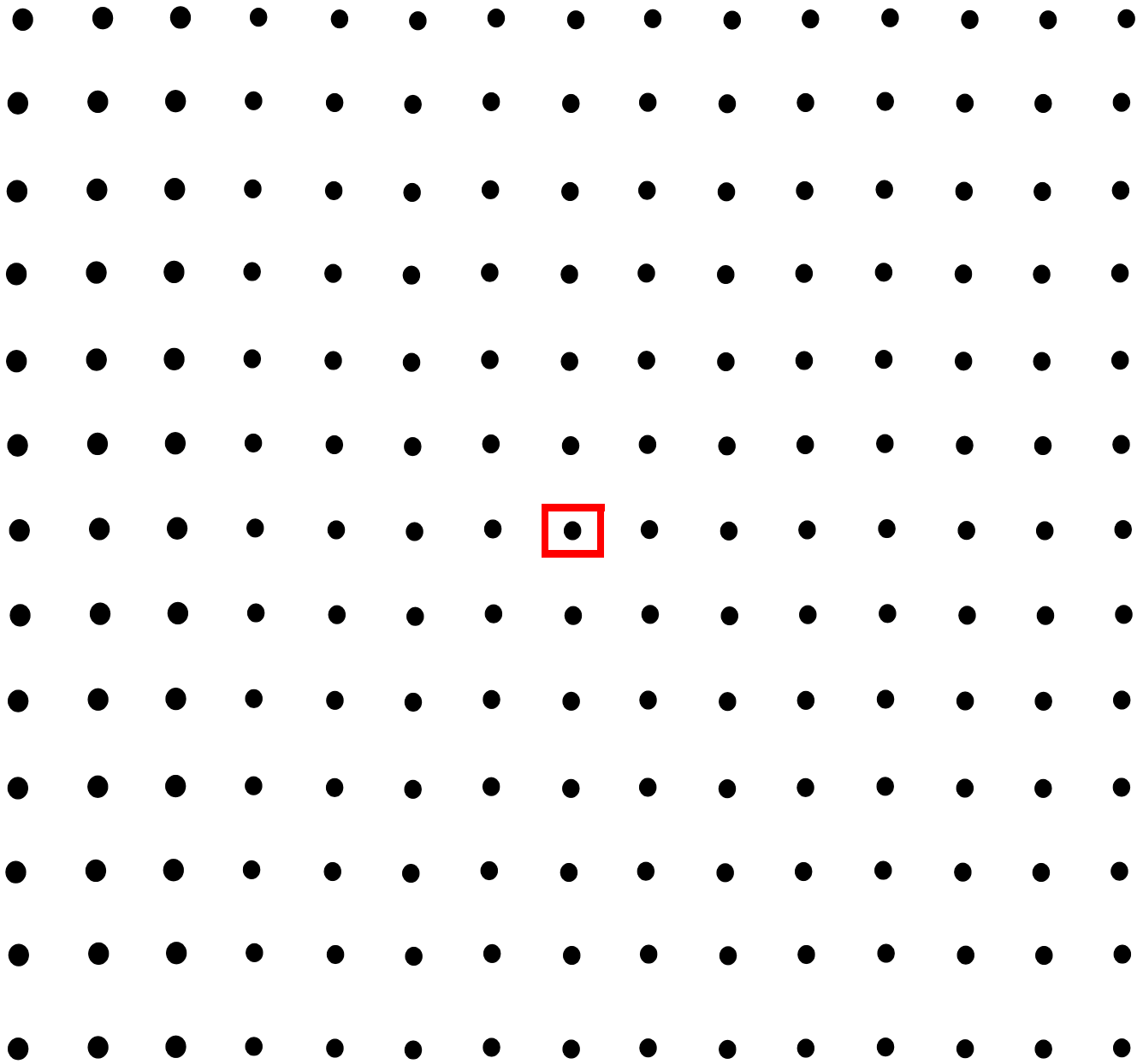

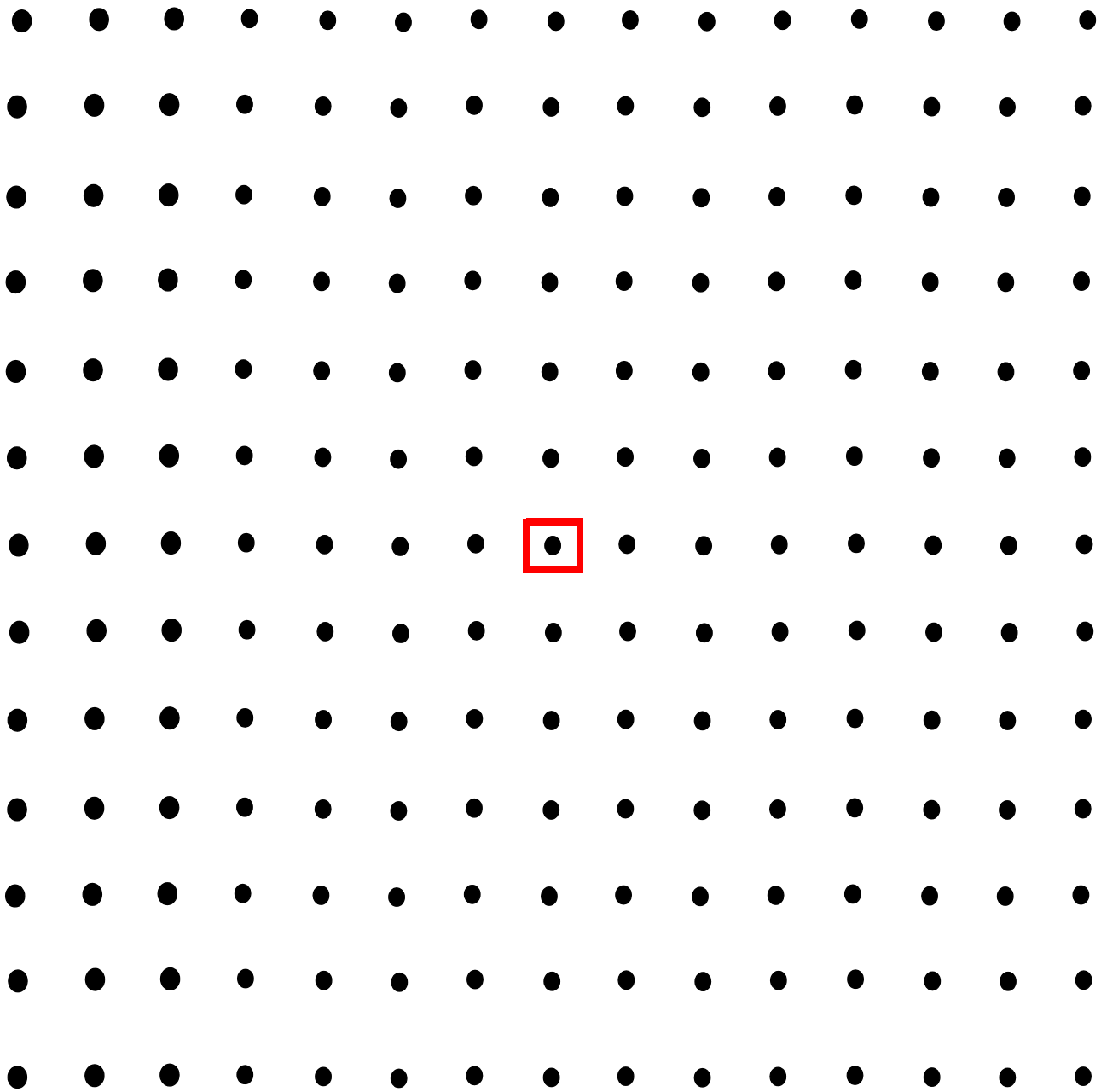

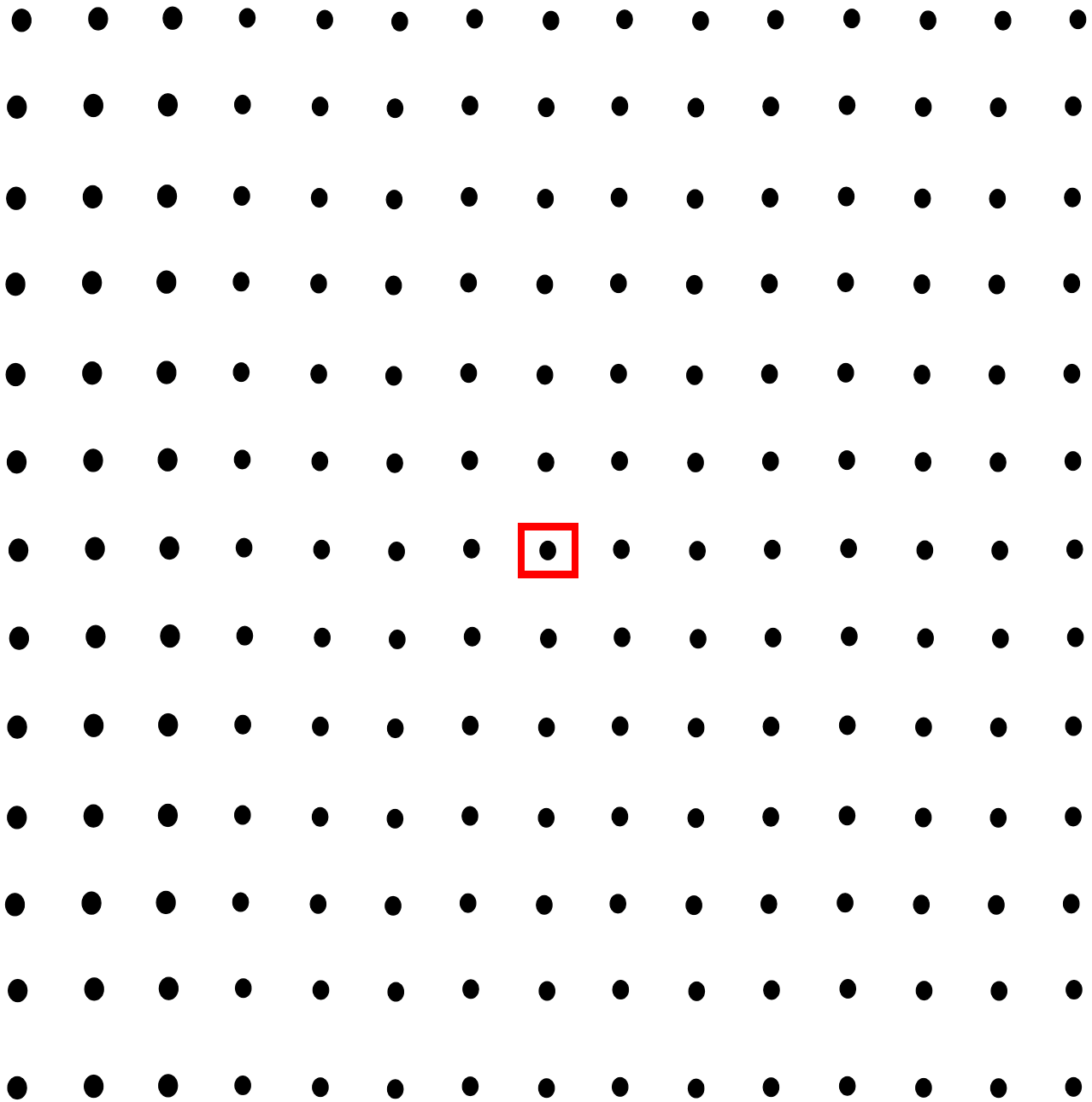

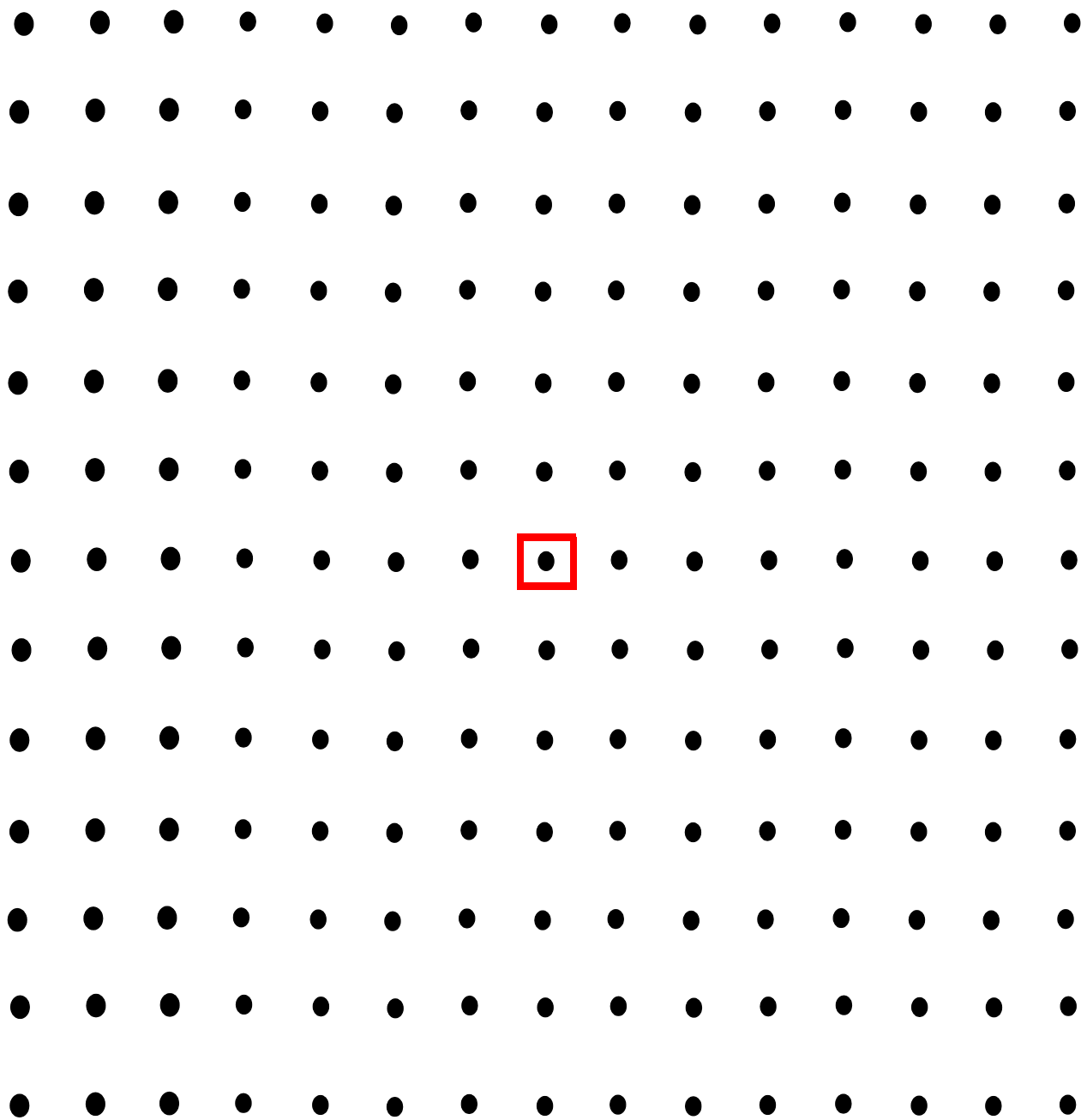

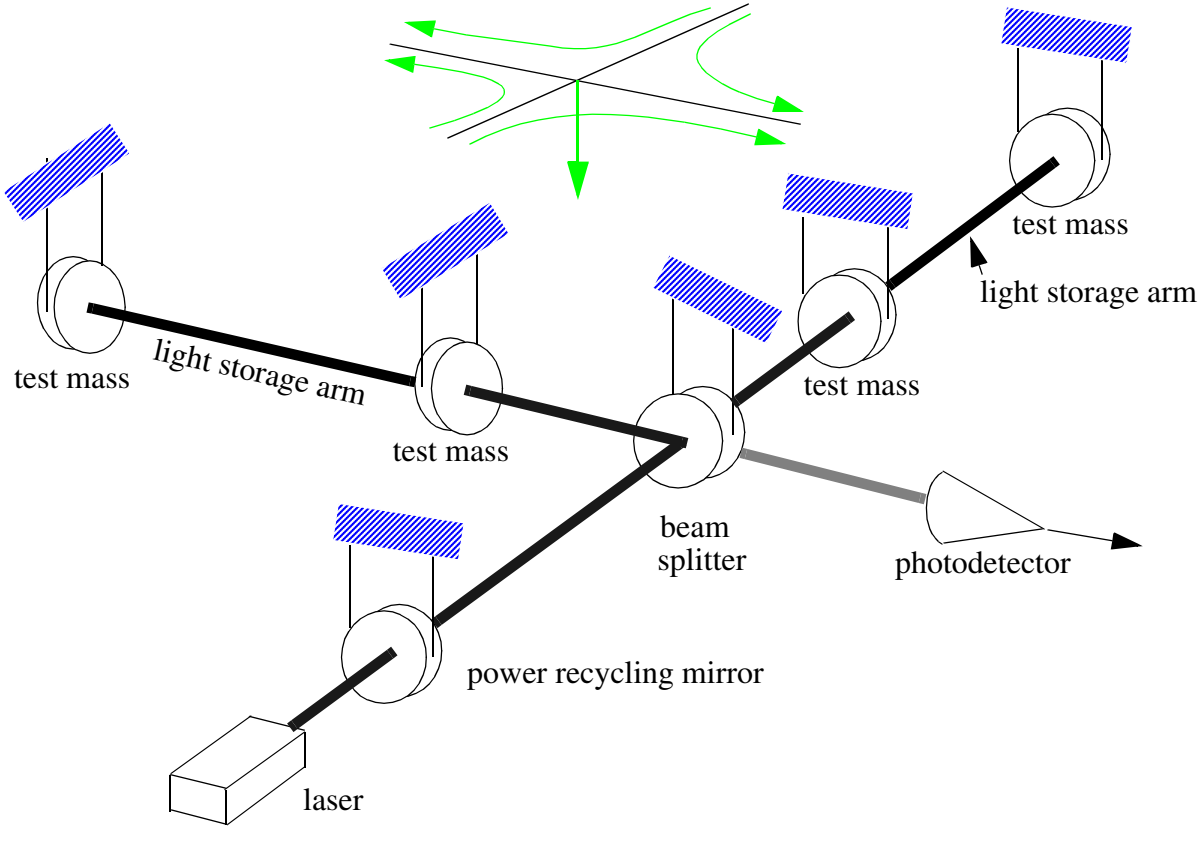
test mass
light storage arm
test mass
test mass
test mass
light storage arm
beam
splitter
photodetector
power recycling mirror
laser

Measurement challenge

- Needed technology development to measure:

$$h = \Delta L/L < 10^{-21}$$

$$\Delta L < 4 \times 10^{-18} \text{ meters}$$

FRINGE SENSING

wavelength 1×10^{-6} m

$$h = \frac{x}{L} \sim \frac{\lambda}{Lb\sqrt{\dot{N}\tau}}$$

arm length = 4000 m

integration time

equivalent # of passes = 100

number of quanta/second at the beam splitter

300 watts at beam splitter = 10^{21} identical photons/sec

$h = 6 \times 10^{-22}$ integration time 10^{-2} sec

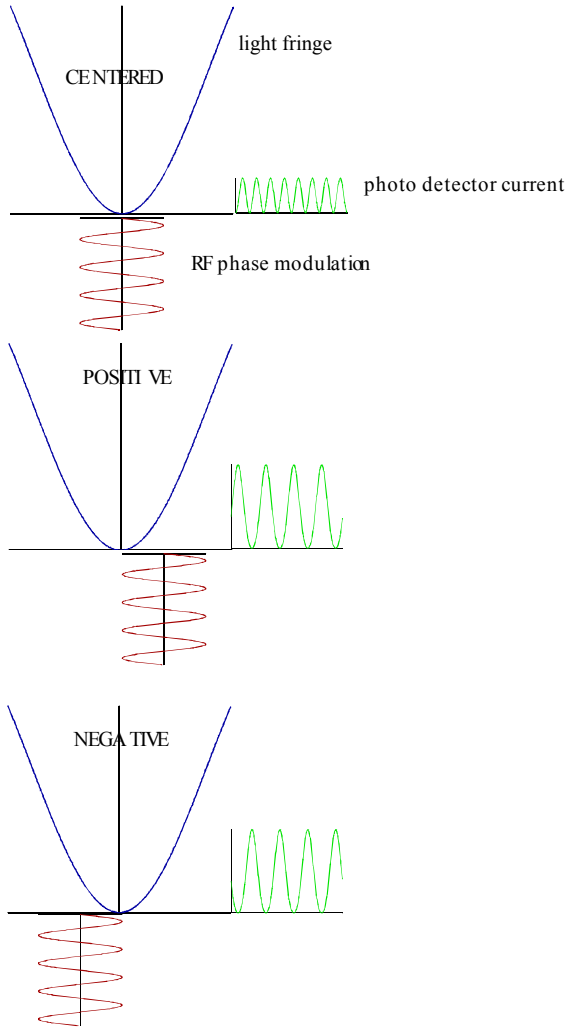

PENDULUM THERMAL NOISE

Pendulum Brownian motion

Dissipation leads to fluctuations

Tc = coherence or damping time
= Q x period of oscillator

Exchange with surroundings:

$$E(\text{thermal}) = \frac{kT\ t}{Tc}$$

Large Tc => smaller fluctuations

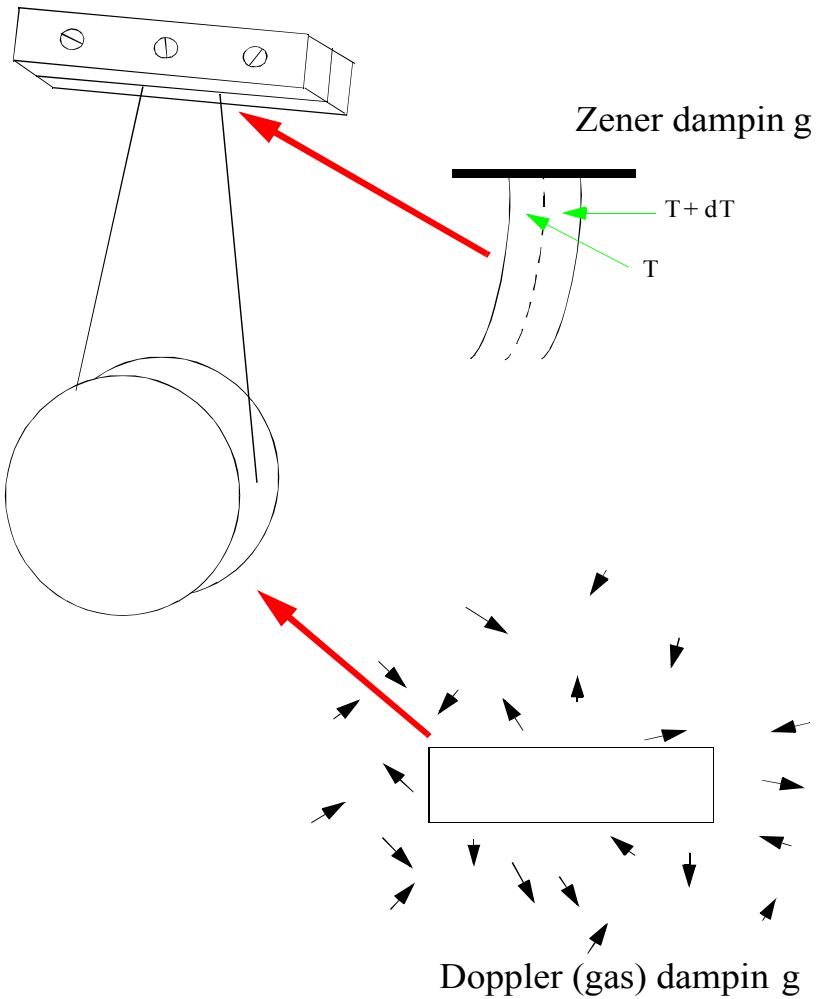

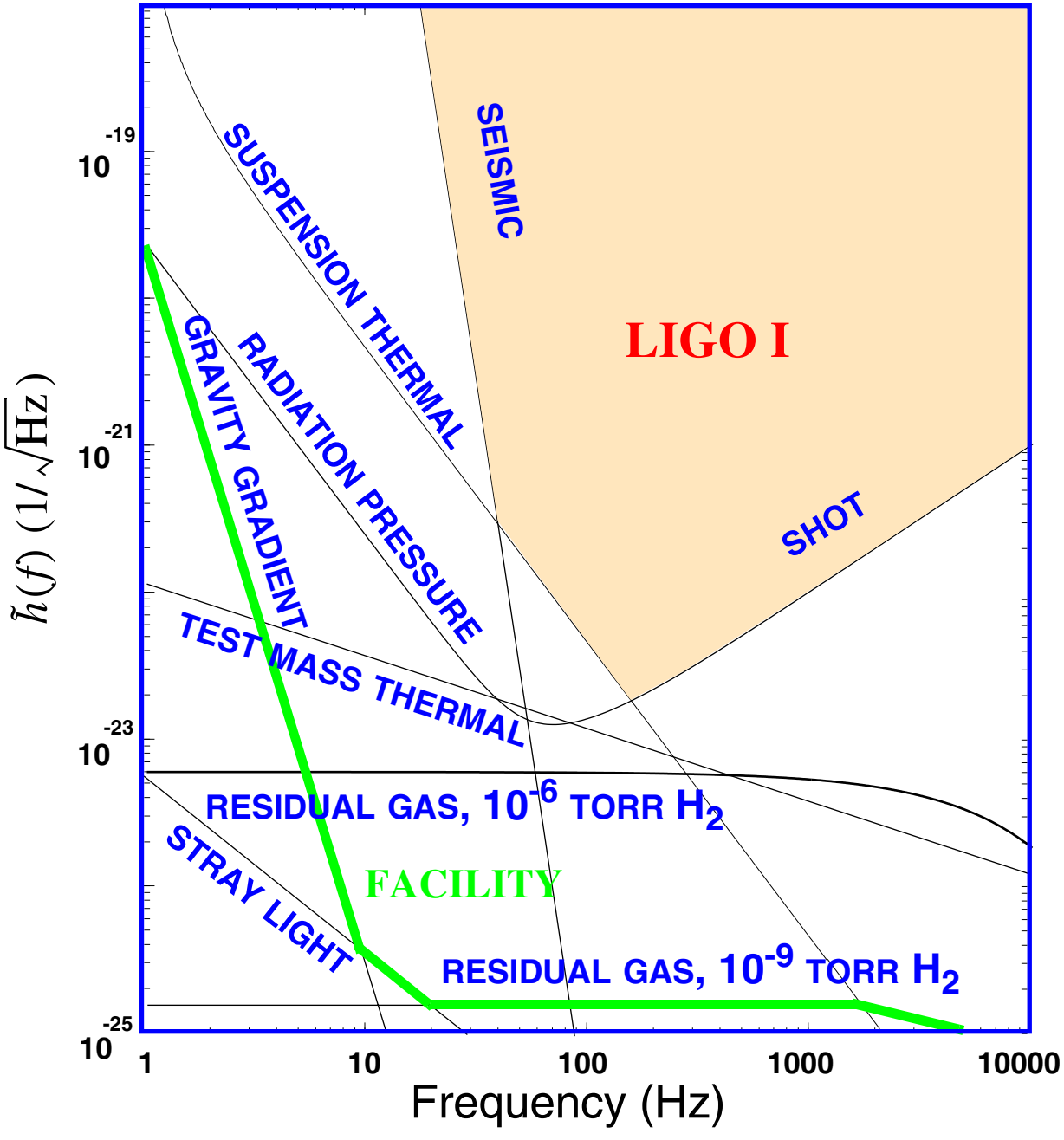
SEISMIC
SUSPENSION THERMAL
RADIATION PRESSURE
GRAVITY GRADIENT
LIGO I
SHOT
TEST MASS THERMAL
RESIDUAL GAS, 10-6 TORR H2
FACILITY
STRAY LIGHT
RESIDUAL GAS, 10-9 TORR H2
10-19
10-21
10-23
10-25
h̃(f) (1/√Hz)
1
10
100
1000
10000
Frequency (Hz)

Interferometers
international network

Simultaneously detect signal (within msec)

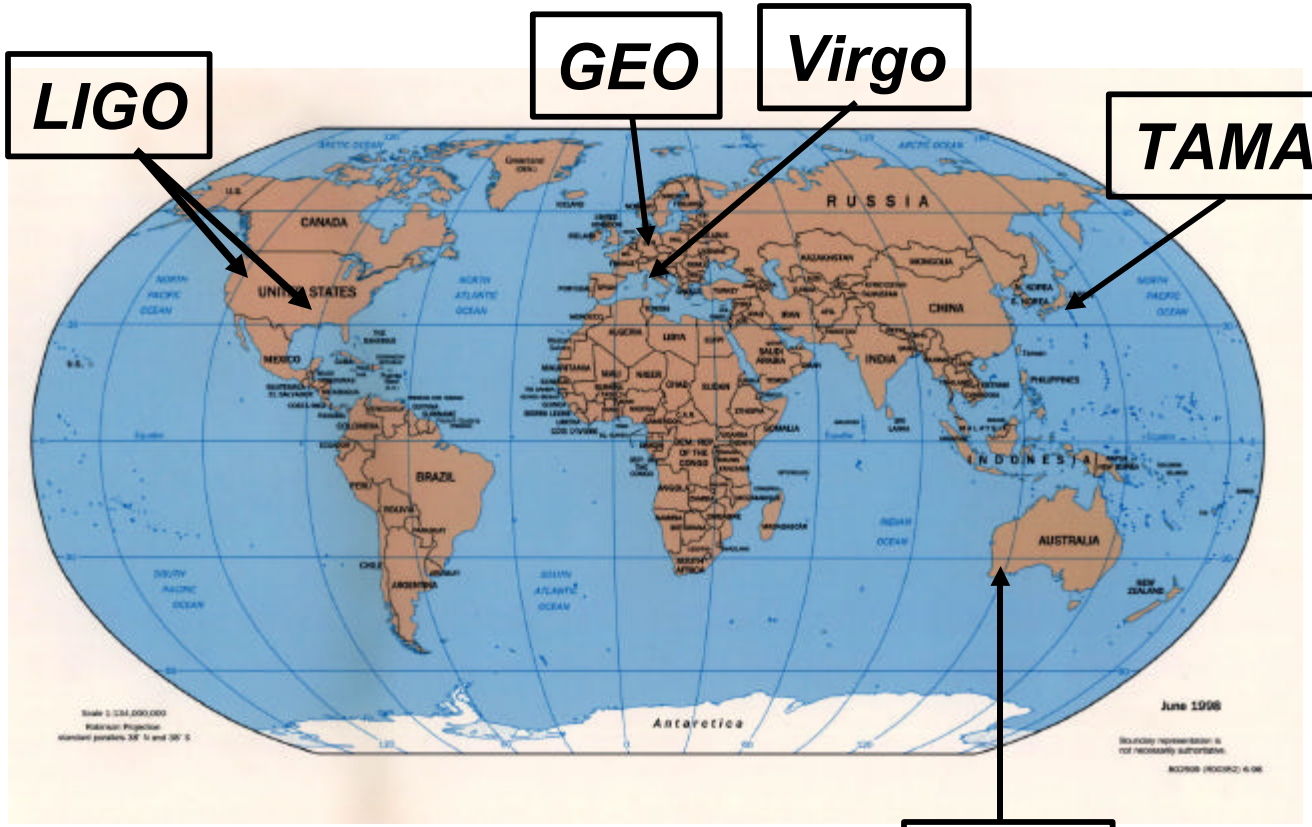

detection confidence

locate the sources

decompose the polarization of gravitational waves

LIGO Observatory Facilities

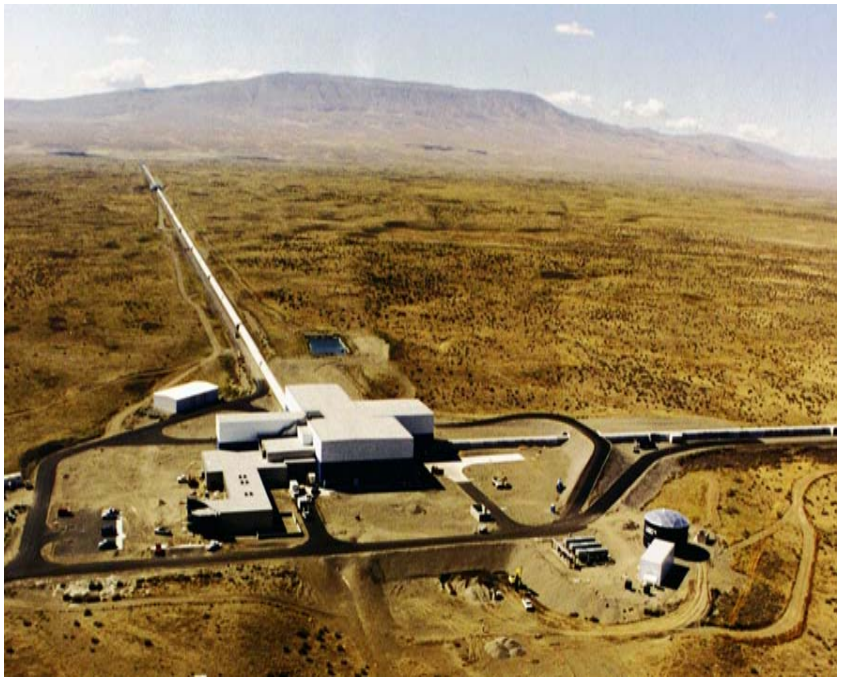

LIGO Hanford Observatory [LHO]

26 km north of Richland, WA

2 km + 4 km interferometers in same vacuum envelope

LIGO Livingston Observatory [LLO]

42 km east of Baton Rouge, LA

Single 4 km interferometer

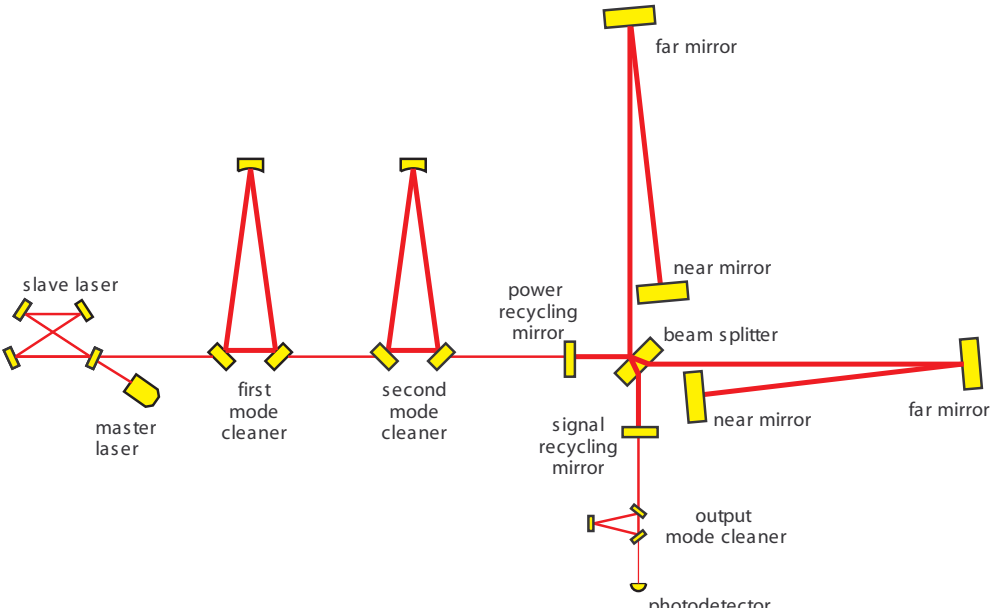
far mirror
near mirror
slave laser
power
recycling
mirror
beam splitter
first
mode
cleaner
second
mode
cleaner
master
laser
near mirror
far mirror
signal
recycling
mirror
output
mode cleaner
photodetector

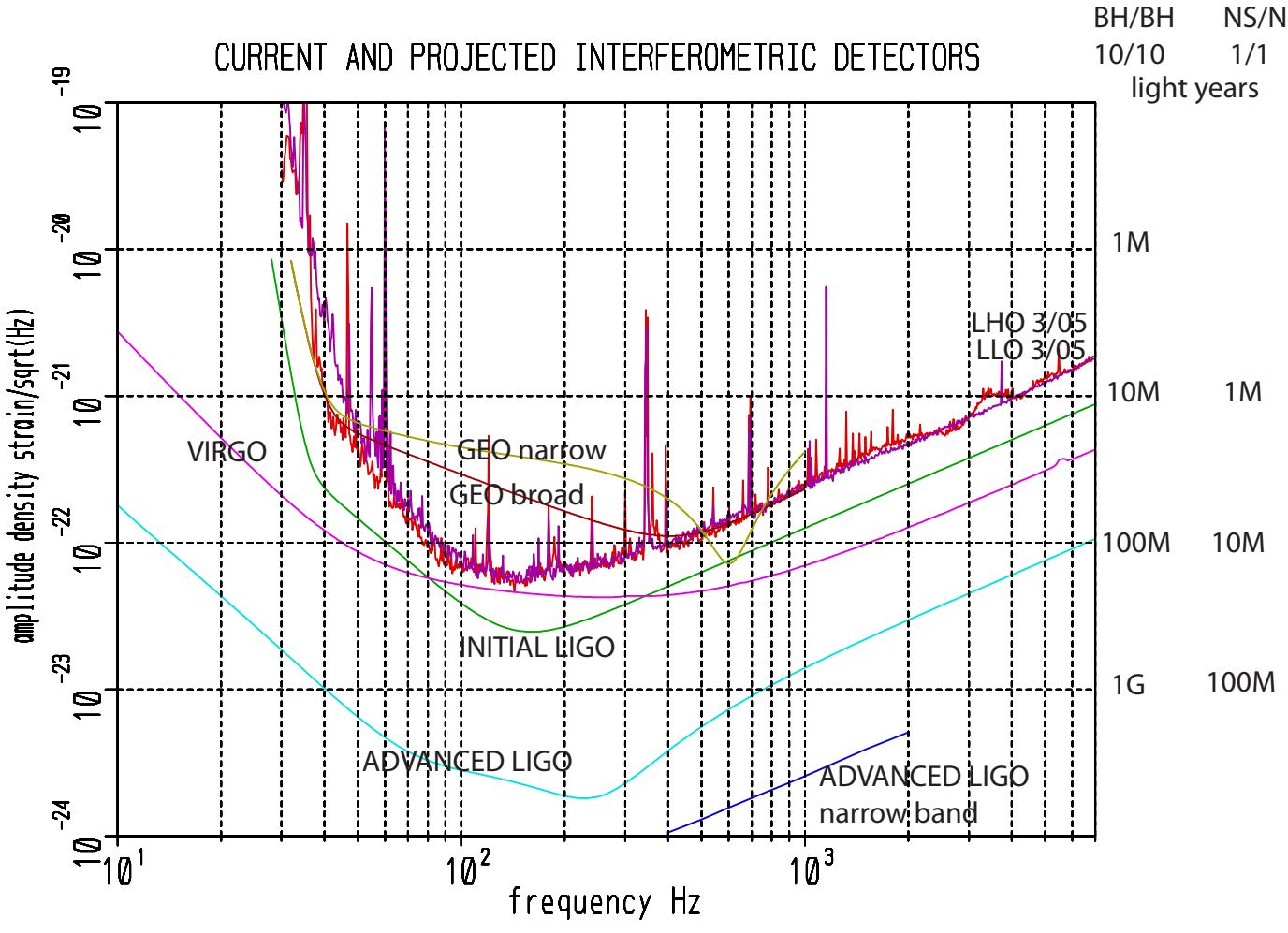
CURRENT AND PROJECTED INTERFEROMETRIC DETECTORS
BH/BH
10/10
NS/NS
1/1
light years
1M
10M
1M
100M
10M
1G
100M
LHO 3/05
LLO 3/05
VIRGO
GEO narrow
GEO broad
INITIAL LIGO
ADVANCED LIGO
ADVANCED LIGO
narrow band
amplitude density strain/sqrt(Hz)
frequency Hz
10^-19
10^-20
10^-21
10^-22
10^-23
10^-24
10^1
10^2
10^3

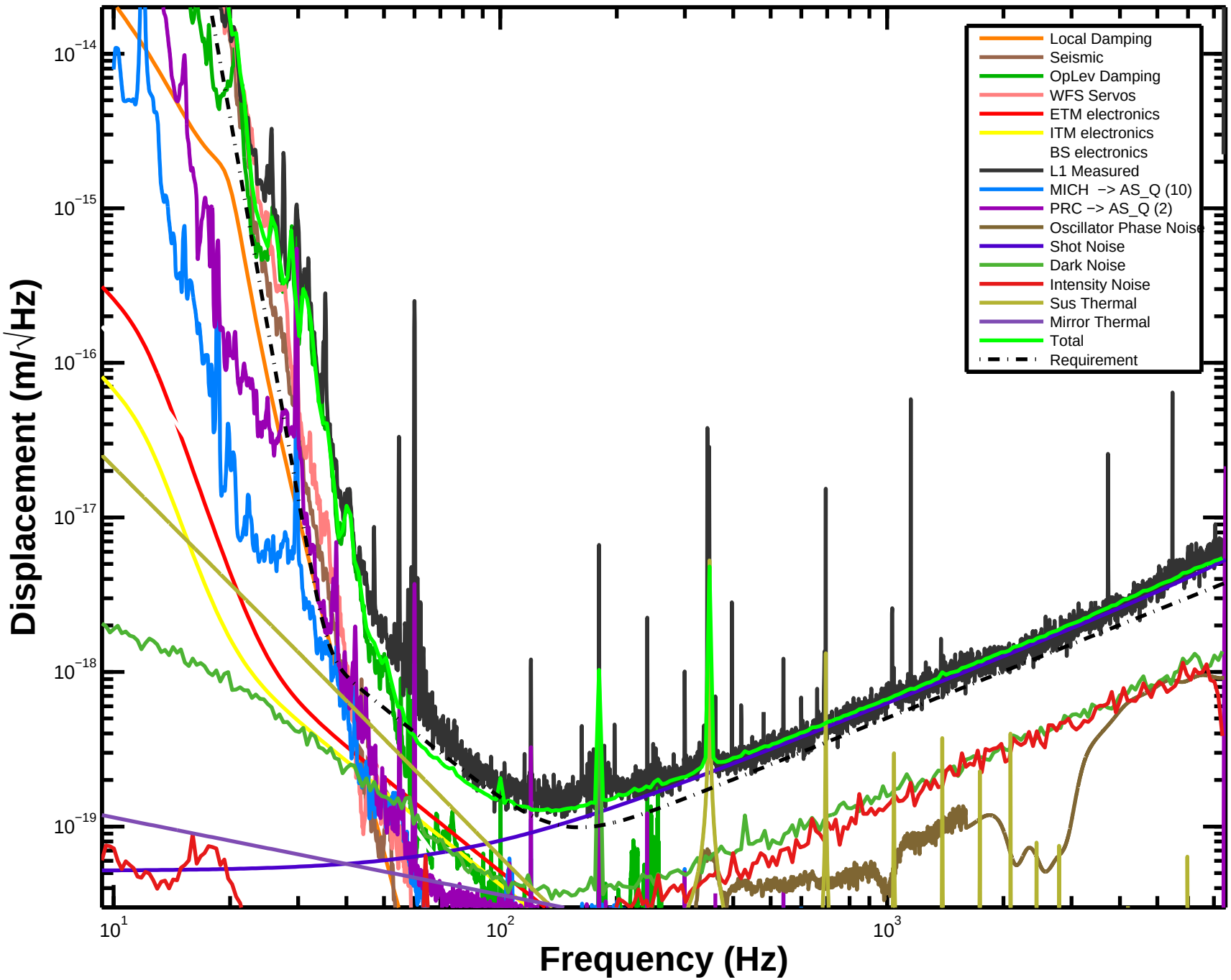
L1: 10.1 Mpc, Apr 20 2005 06:01:38 UTC
Displacement (m/√Hz)
Frequency (Hz)
Local Damping
Seismic
OpLev Damping
WFS Servos
ETM electronics
ITM electronics
BS electronics
L1 Measured
MICH −> AS_Q (10)
PRC −> AS_Q (2)
Oscillator Phase Noise
Shot Noise
Dark Noise
Intensity Noise
Sus Thermal
Mirror Thermal
Total
Requirement

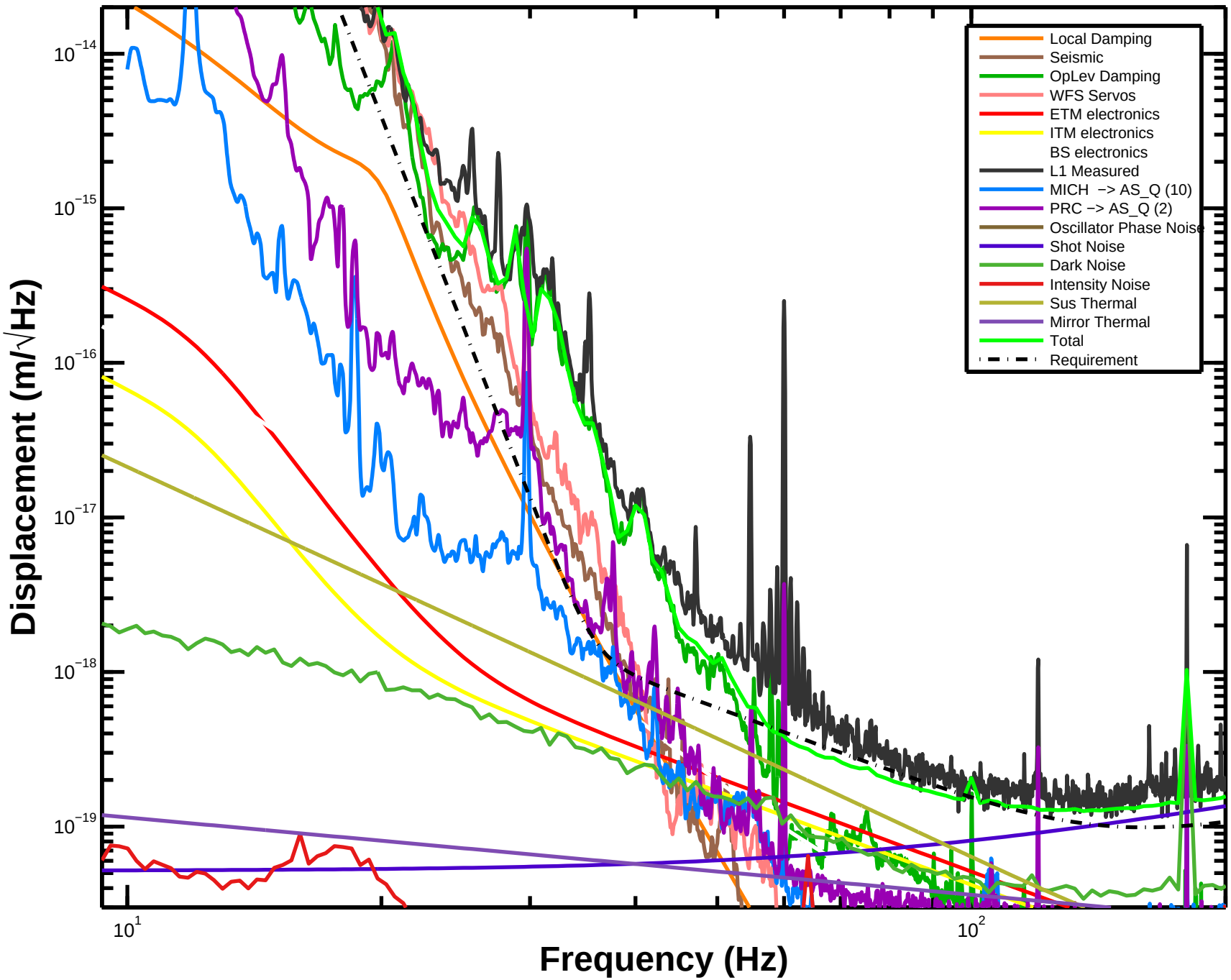
L1: 10.1 Mpc, Apr 20 2005 06:01:38 UTC
Displacement (m/√Hz)
Frequency (Hz)
10^{-14}
10^{-15}
10^{-16}
10^{-17}
10^{-18}
10^{-19}
10^{1}
10^{2}
Local Damping
Seismic
OpLev Damping
WFS Servos
ETM electronics
ITM electronics
BS electronics
L1 Measured
MICH −> AS_Q (10)
PRC −> AS_Q (2)
Oscillator Phase Noise
Shot Noise
Dark Noise
Intensity Noise
Sus Thermal
Mirror Thermal
Total
Requirement

Gravitational Radiation and Detectors:
LIGO Sensitivity Improvements

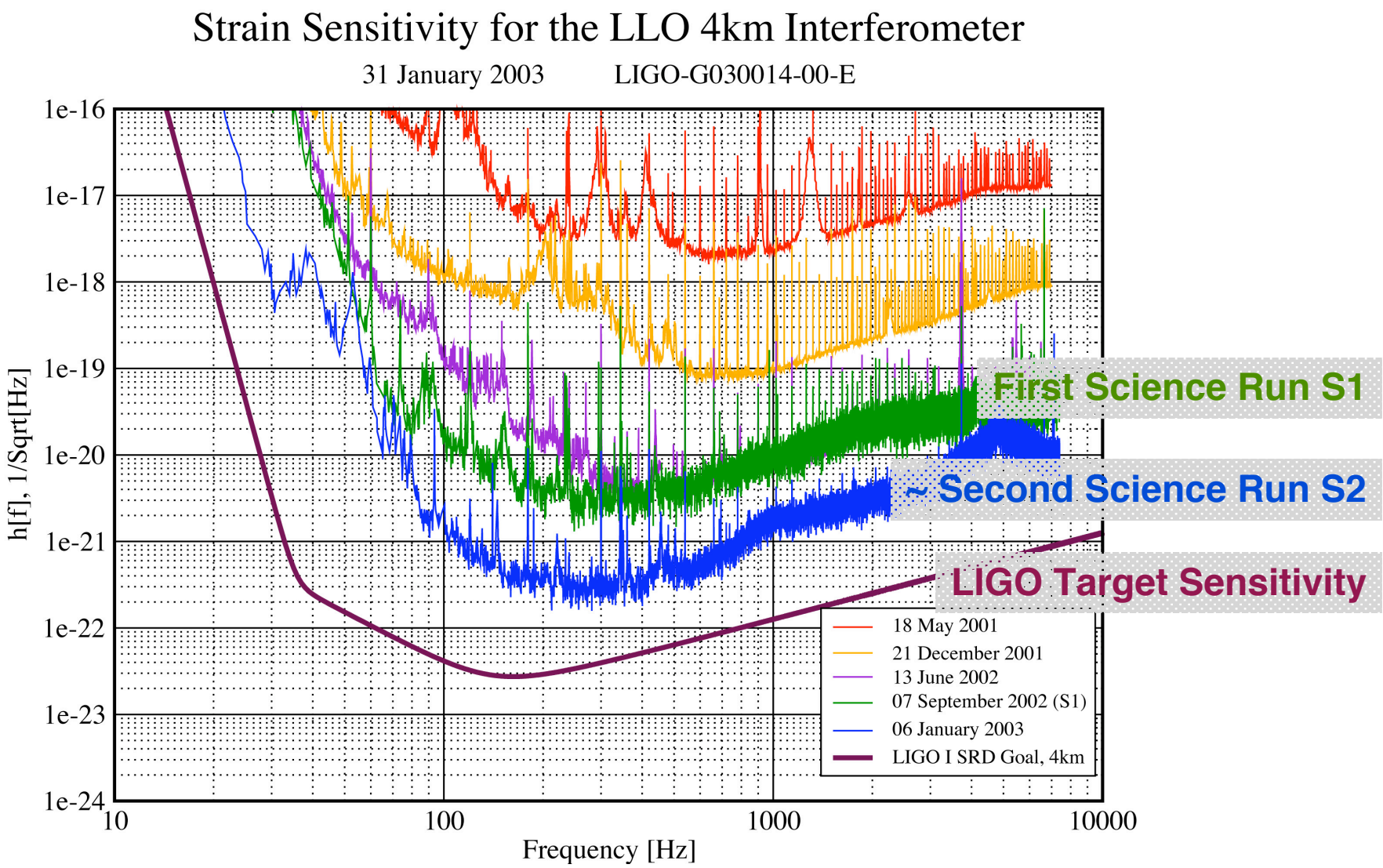

Classes of sources

- Compact binary inspiral: template search
  - BH/BH
  - NS/NS and BH/NS
- Low duty cycle transients: wavelets,T/f clusters
  - Supernova
  - BH normal modes
  - Unknown types of sources
- Periodic CW sources
  - Pulsars
  - Low mass x-ray binaries (quasi periodic)
- Stochastic background
  - Foreground sources : gravitational wave radiometry
  - Cosmological isotropic background

Rate < 47 inspirals/yr/milky way galaxy to a distance of 1.5Mpc
Mass range 1 to 3 solar masses

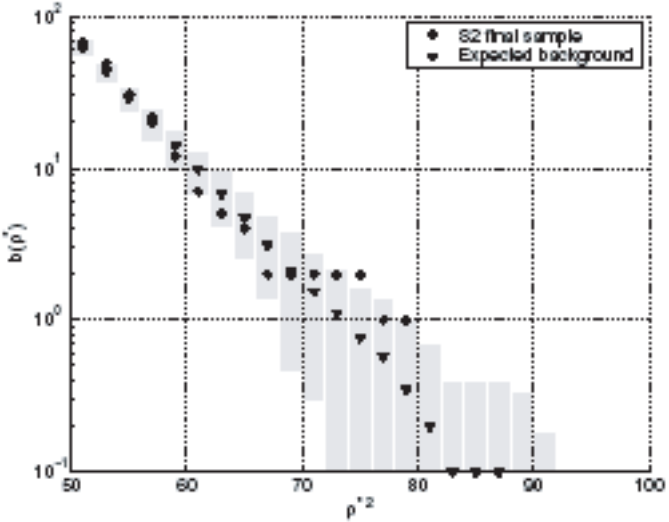

FIG. 10: The mean number of triggers per S2 above SNR ρ^* using the best fit clustering method. The triangles represent the expected background. See Fig. 8 and Sec. VII for details of the time-shifts and for comparison with largest SNR clustering. We note that there is no apparent excess of S2 coincident triggers over the expected background from accidental coincidences in this plot.

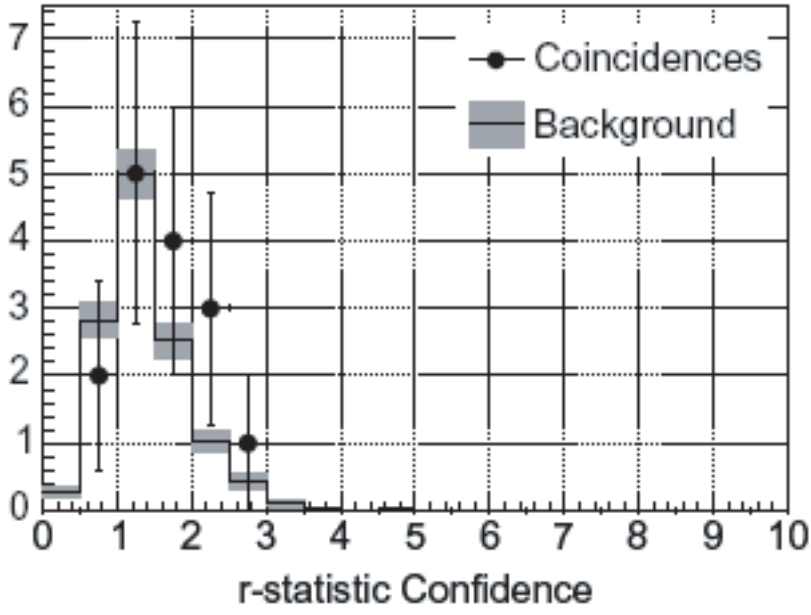

FIG. 7: Histogram of r-statistic confidence values (Γ's), for events passing the WaveBurst analysis at zero-lag (shown with circles) and at time-shifts (*i.e.*, background, shown with bars), after applying the acoustic veto. The histogram of background events is normalized to the live-time of the zero-lag analysis.

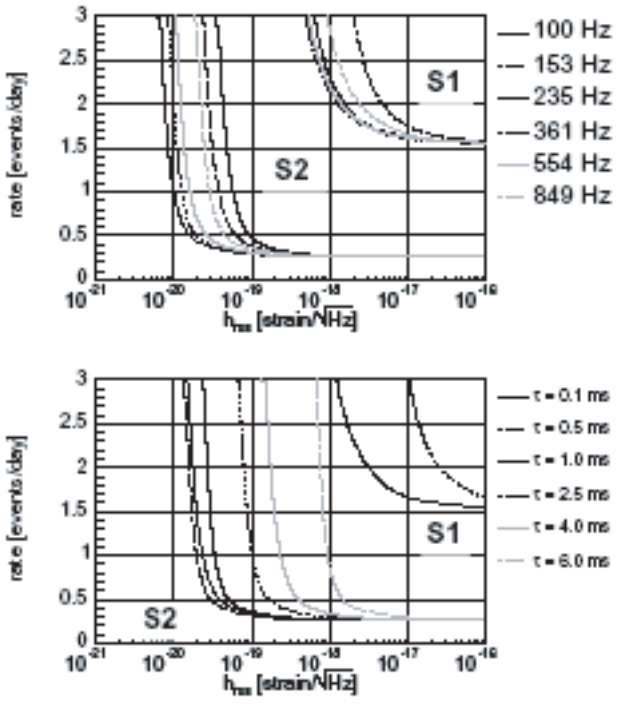

FIG. 12: Rate versus h_{rss} exclusion plots at the 90% confidence level derived from the LIGO burst search using the S2 data. The top plot corresponds to burst events modeled by sine-Gaussians of $Q = 8.9$ and frequencies ranging from 100 Hz to 850 Hz, while the bottom plot corresponds to ones events modeled by Gaussians of the τ's shown. For comparison, the corresponding curves resulting from the S1 analysis are superimposed.

pulsar	spin f (Hz)	spindown $\dot{f}$ (Hz s^{-1})	$h_0^{95\%}$ $/10^{-24}$	ϵ $/10^{-5}$
B0021−72C*	173.71	$+1.50\times10^{-15}$	4.3	16
B0021−72D*	186.65	$+1.19\times10^{-16}$	4.1	14
B0021−72F*	381.16	-9.37×10^{-15}	7.2	5.7
B0021−72G*	247.50	$+2.58\times10^{-15}$	4.1	7.5
B0021−72L*	230.09	$+6.46\times10^{-15}$	2.9	6.1
B0021−72M*	271.99	$+2.84\times10^{-15}$	3.3	5.0
B0021−72N*	327.44	$+2.34\times10^{-15}$	4.0	4.3
J0030+0451	205.53	-4.20×10^{-16}	3.8	0.48
B0531+21*	29.81	-3.74×10^{-10}	41	2 100
J0711−6830	182.12	-4.94×10^{-16}	2.4	1.8
J1024−0719*	193.72	-6.95×10^{-16}	3.9	0.86
B1516+02A	180.06	-1.34×10^{-15}	3.6	21
J1629−6902	166.65	-2.78×10^{-16}	2.3	2.7
J1721−2457	285.99	-4.80×10^{-16}	4.0	1.8
J1730−2304*	123.11	-3.06×10^{-16}	3.1	2.5
J1744−1134*	245.43	-5.40×10^{-16}	5.9	0.83
J1748−2446C	118.54	$+8.52\times10^{-15}$	3.1	24
B1820−30A*	183.82	-1.14×10^{-13}	4.2	24
B1821−24*	327.41	-1.74×10^{-13}	5.6	7.1
J1910−5959B	119.65	$+1.14\times10^{-14}$	2.4	8.5
J1910−5959C	189.49	-7.90×10^{-17}	3.3	4.7
J1910−5959D	110.68	-1.18×10^{-14}	1.7	7.2
J1910−5959E	218.73	$+2.09\times10^{-14}$	7.5	7.9
J1913+1011*	27.85	-2.61×10^{-12}	51	6 900
J1939+2134*	641.93	-4.33×10^{-14}	13	2.7
B1951+32*	25.30	-3.74×10^{-12}	48	4 400
J2124−3358*	202.79	-8.45×10^{-16}	3.1	0.45
J2322+2057*	207.97	-4.20×10^{-16}	4.1	1.8

TABLE I: The 28 pulsars targeted in the S2 run, with approximate spin parameters. Pulsars for which radio timing data were taken over the S2 period are starred (*). The right-hand two columns show the 95% upper limit on h_0, based on a coherent analysis using all the S2 data, and corresponding ellipticity values (ϵ, see text). These upper limit values do *not* include the uncertainties due to calibration and to pulsar timing accuracy, which are discussed in the text, nor uncertainties in the pulsar's distance, r.

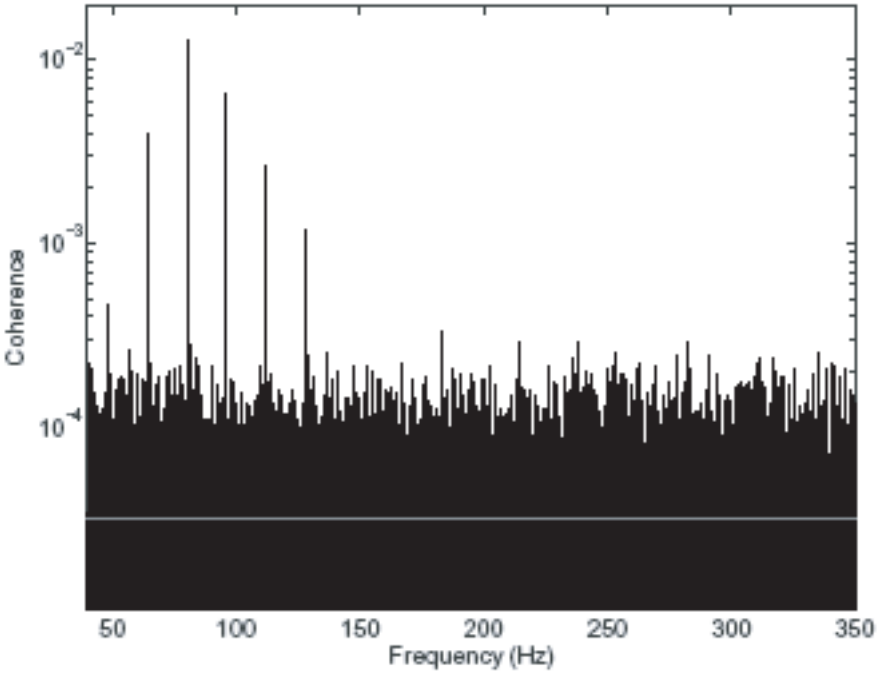

FIG. 2: Coherence between the H1 and L1 detector outputs during S3, showing a few small, but significant, coherent peaks at multiples of 16 Hz. The grey line corresponds to the expected statistical uncertainty level of $1/N_{\rm avg} \approx 3 \times 10^{-5}$.

Overlap reduction function

Specifies the reduction in sensitivity due to the separation and orientation of the two detectors:

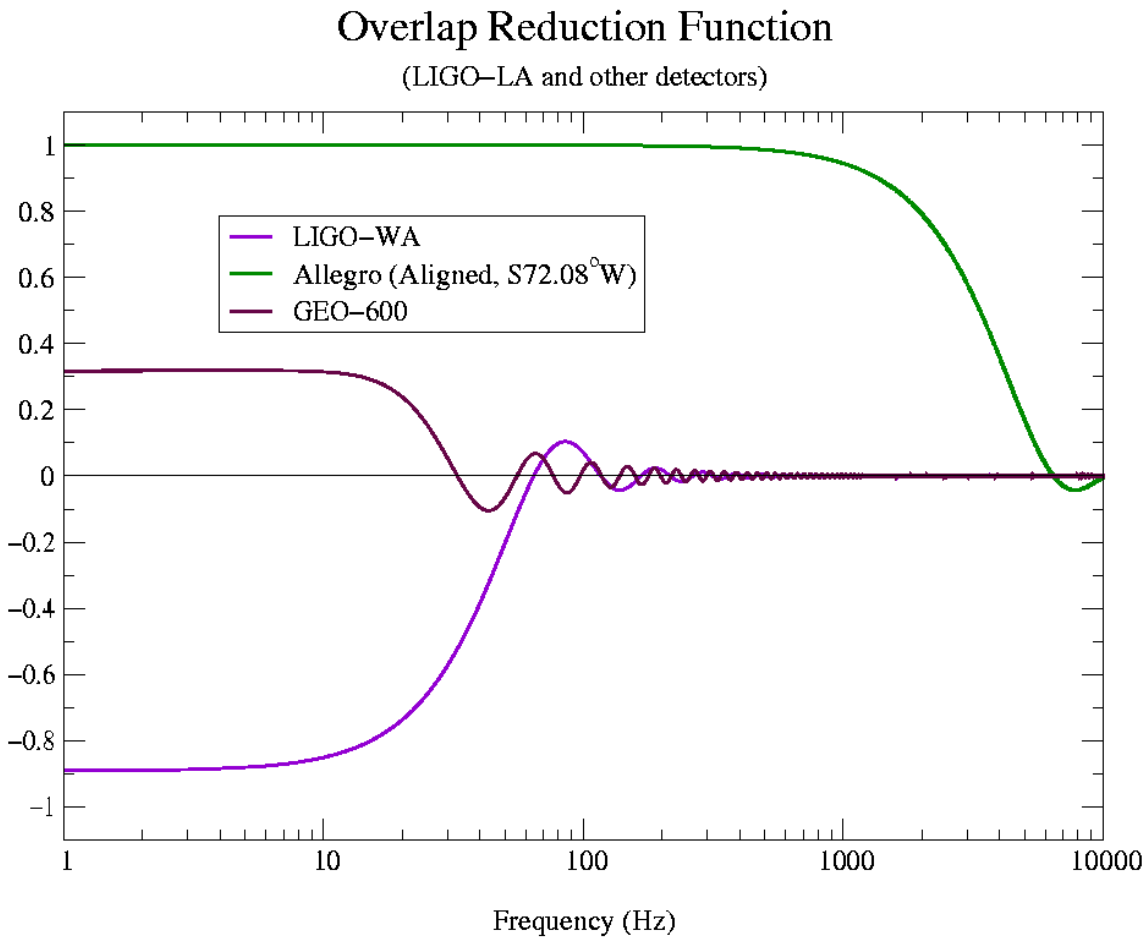

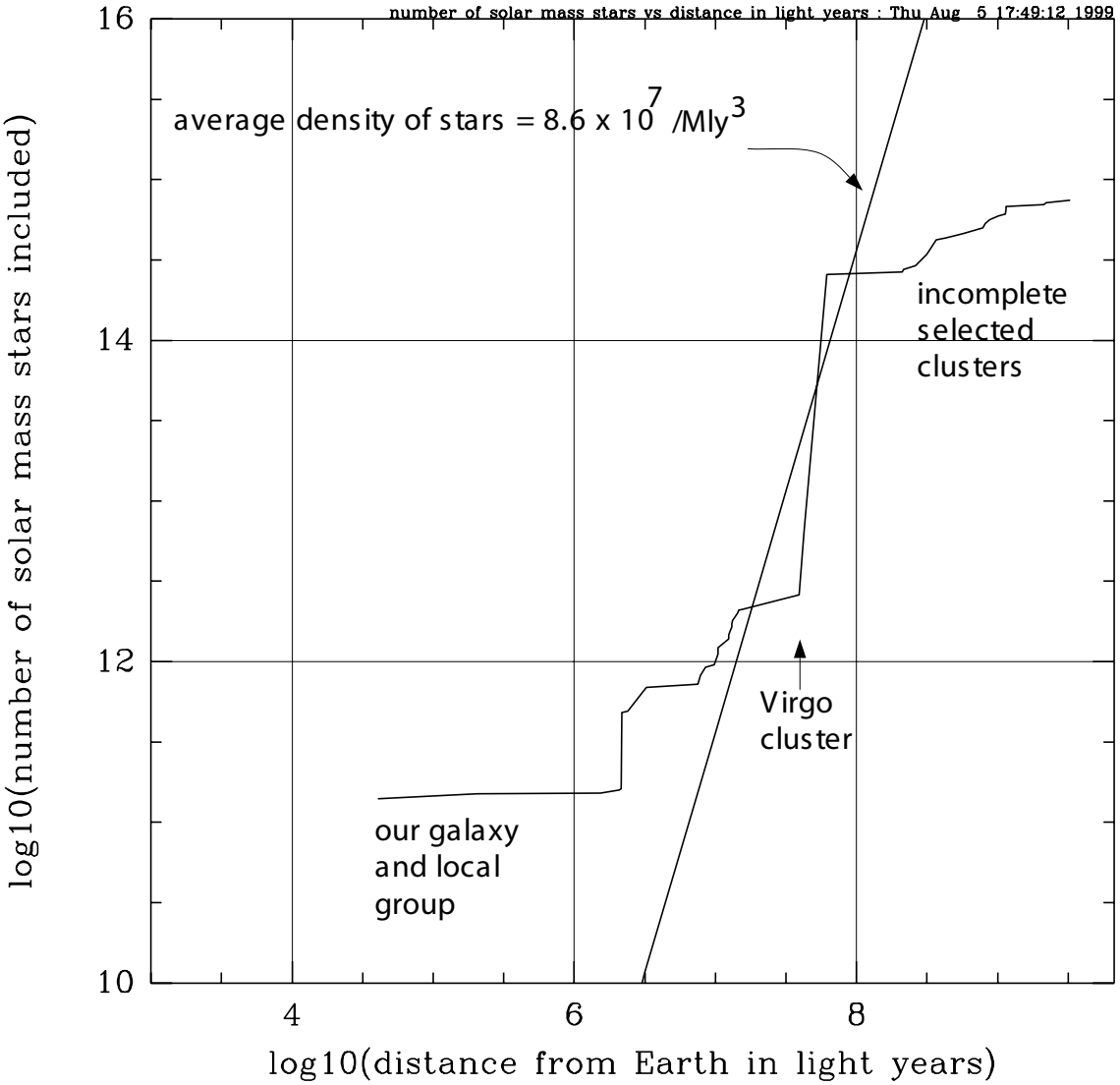

DATA: Cosmology of the Local Group G.Lake
Astrophysical Quantities C.W. Allen

Binary Coalescence Sources & Science:
Binary Neutron Stars: S1 Range

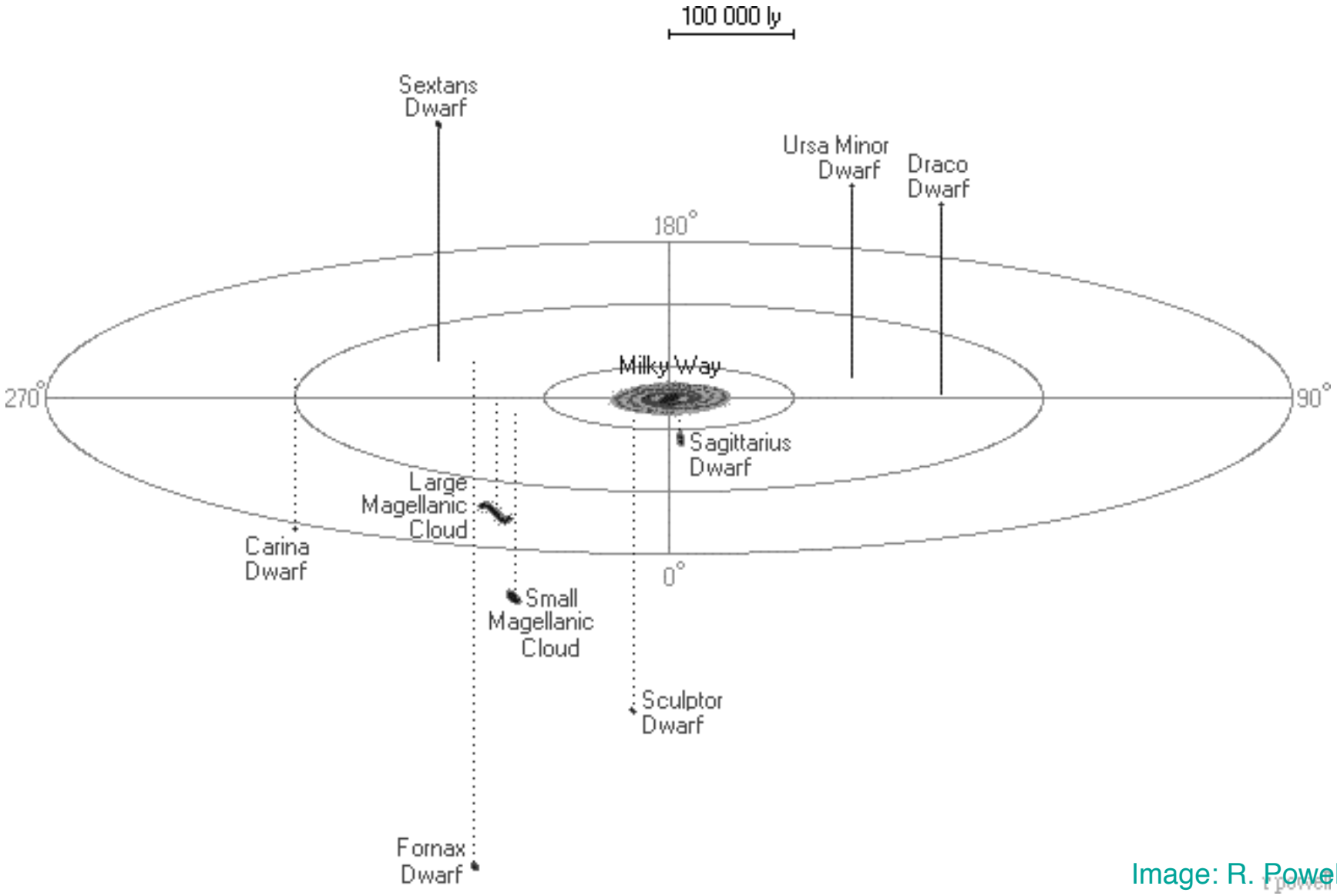

Image: R. Powell

Binary Coalescence Sources & Science:

Binary Neutron Stars: S2 Range

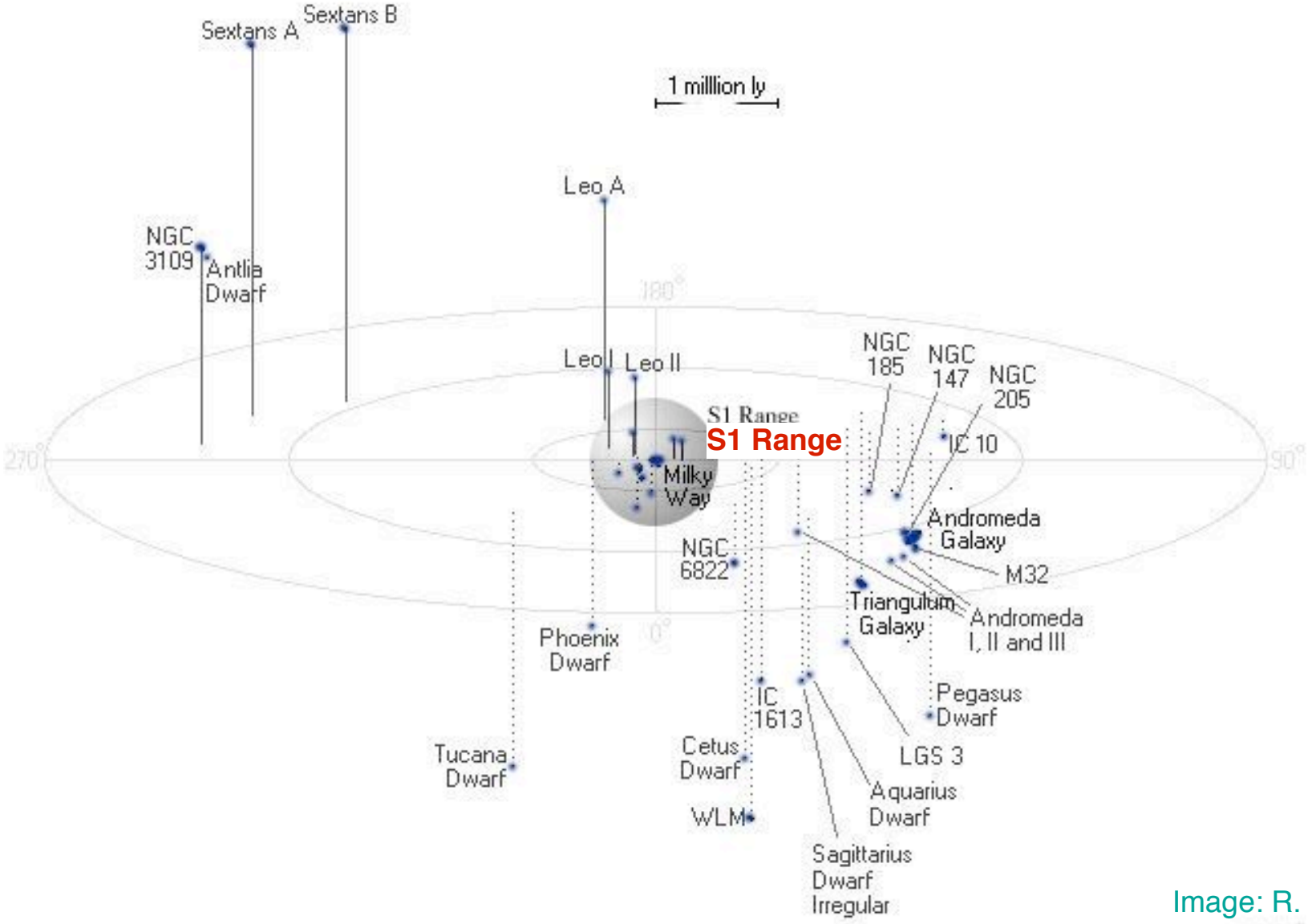

Image: R. Powell

Binary Coalescence Sources & Science:
Binary Neutron Stars: LIGO Range

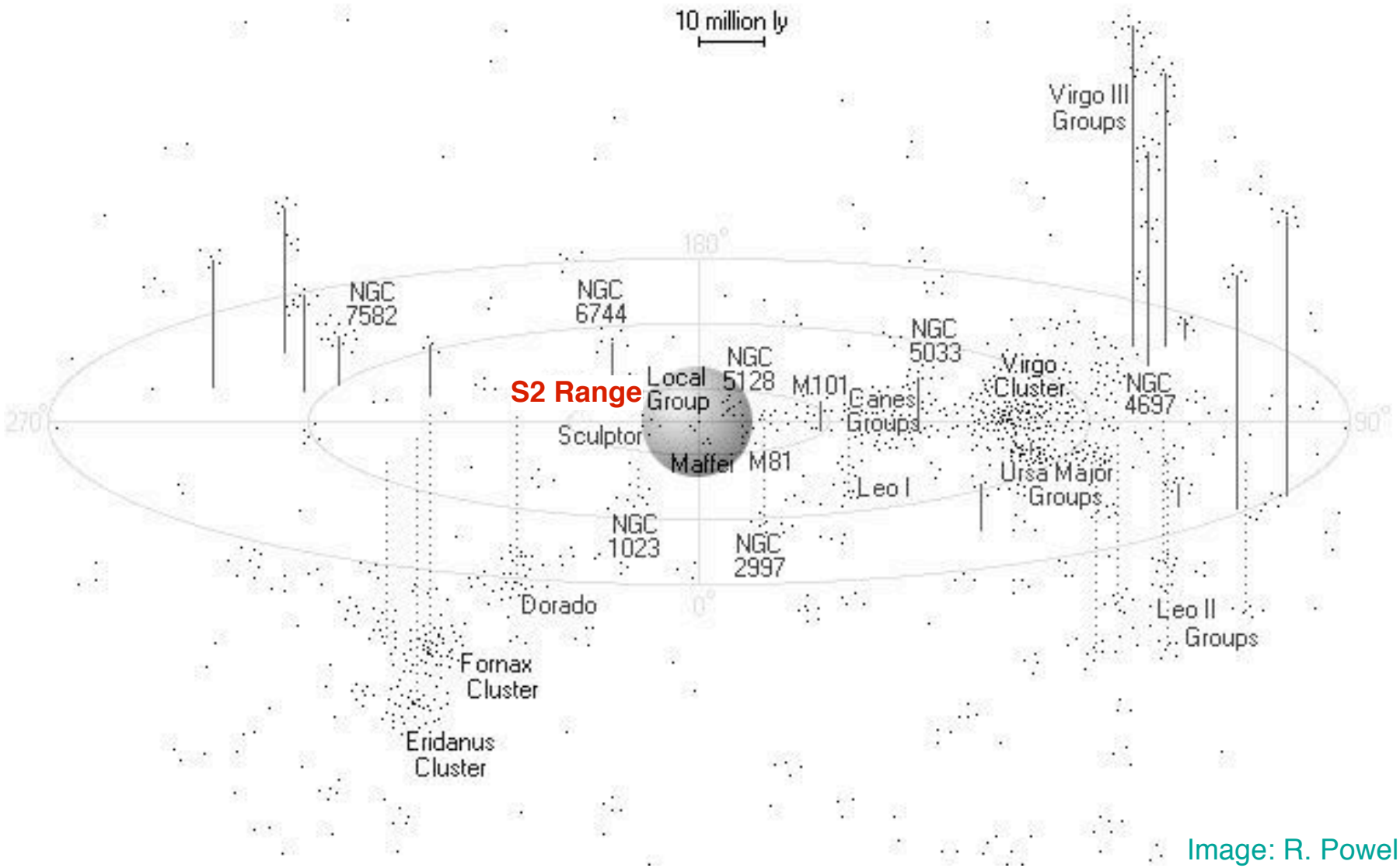

Image: R. Powell

Binary Coalescence Sources & Science:
Binary Neutron Stars: AdLIGO Range

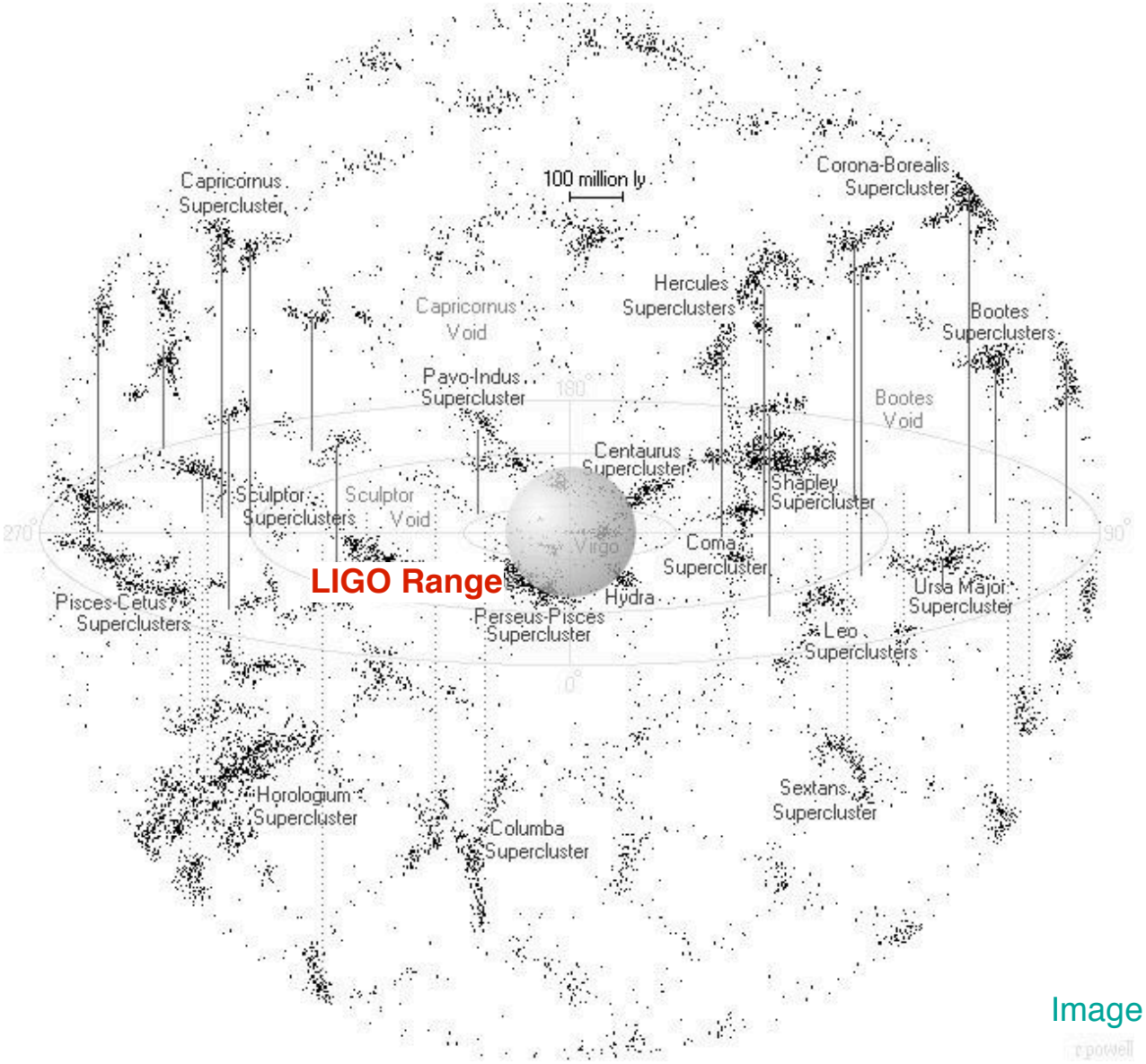

Image: R. Powell

Advanced Interferometer Concept

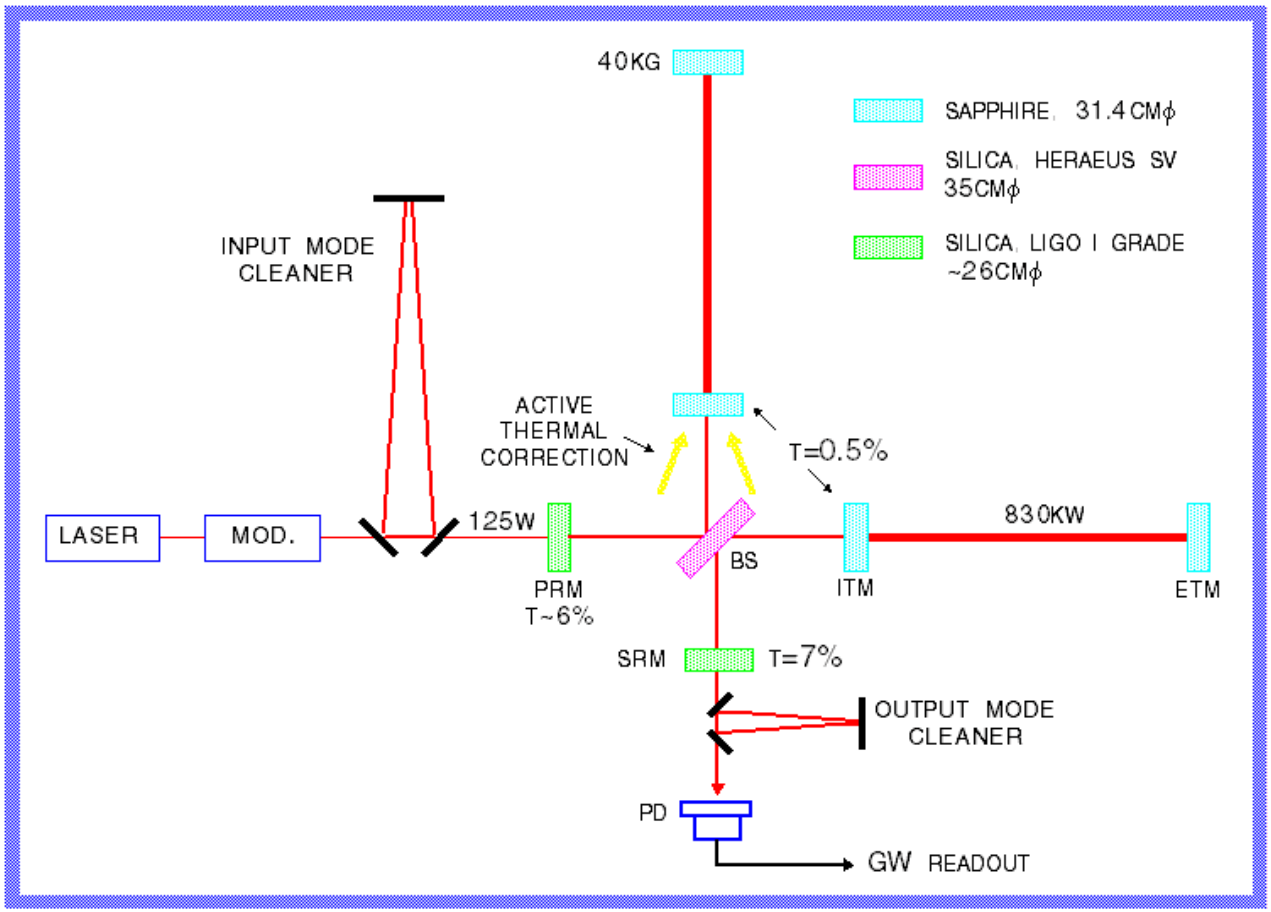

- » Signal recycling
- » 180-watt laser
- » 40 kg Sapphire test masses
- » Larger beam size
- » Quadruple suspensions
- » Active seismic isolation
- » Active thermal correction
- » Output mode cleaner

Projected Performance

- Seismic ‘cutoff’ at 10 Hz
- Suspension thermal noise
- Internal thermal noise
- Unified quantum noise dominates at most frequencies
- ‘technical’ noise (e.g., laser frequency) levels held in general well below these ‘fundamental’ noises

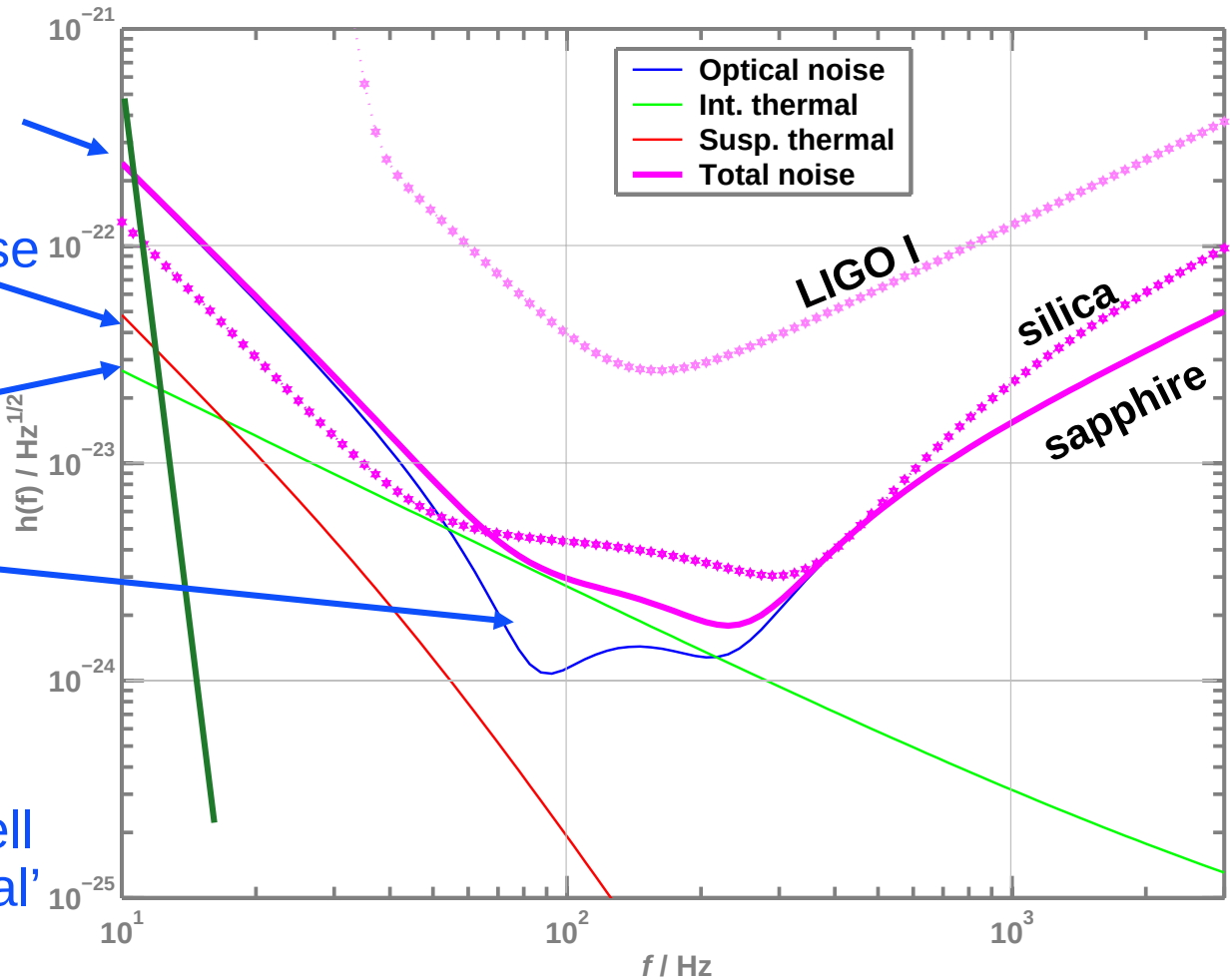

The Gravitational-Wave Spectrum

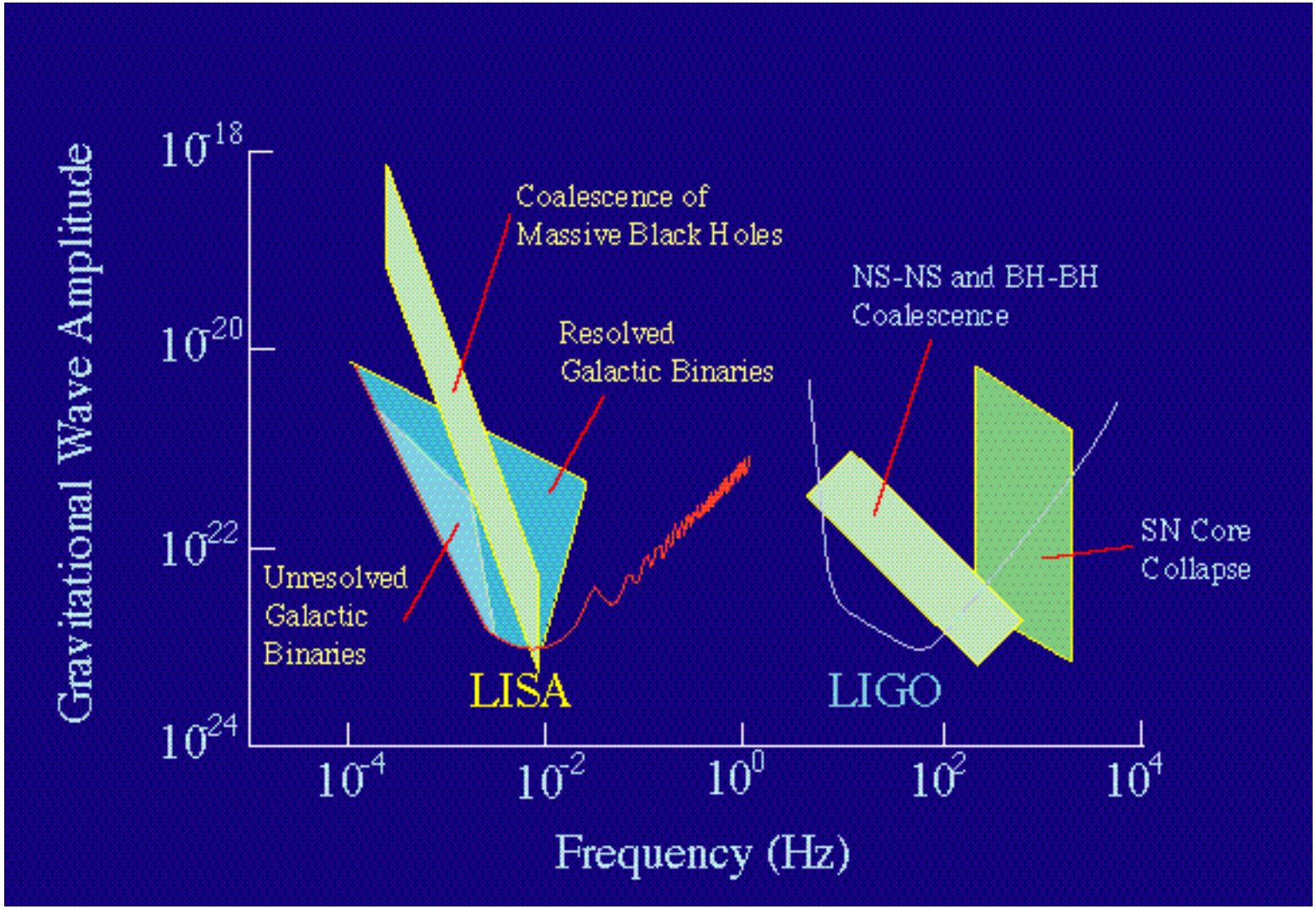

Massive Black Holes in Merging Galaxies

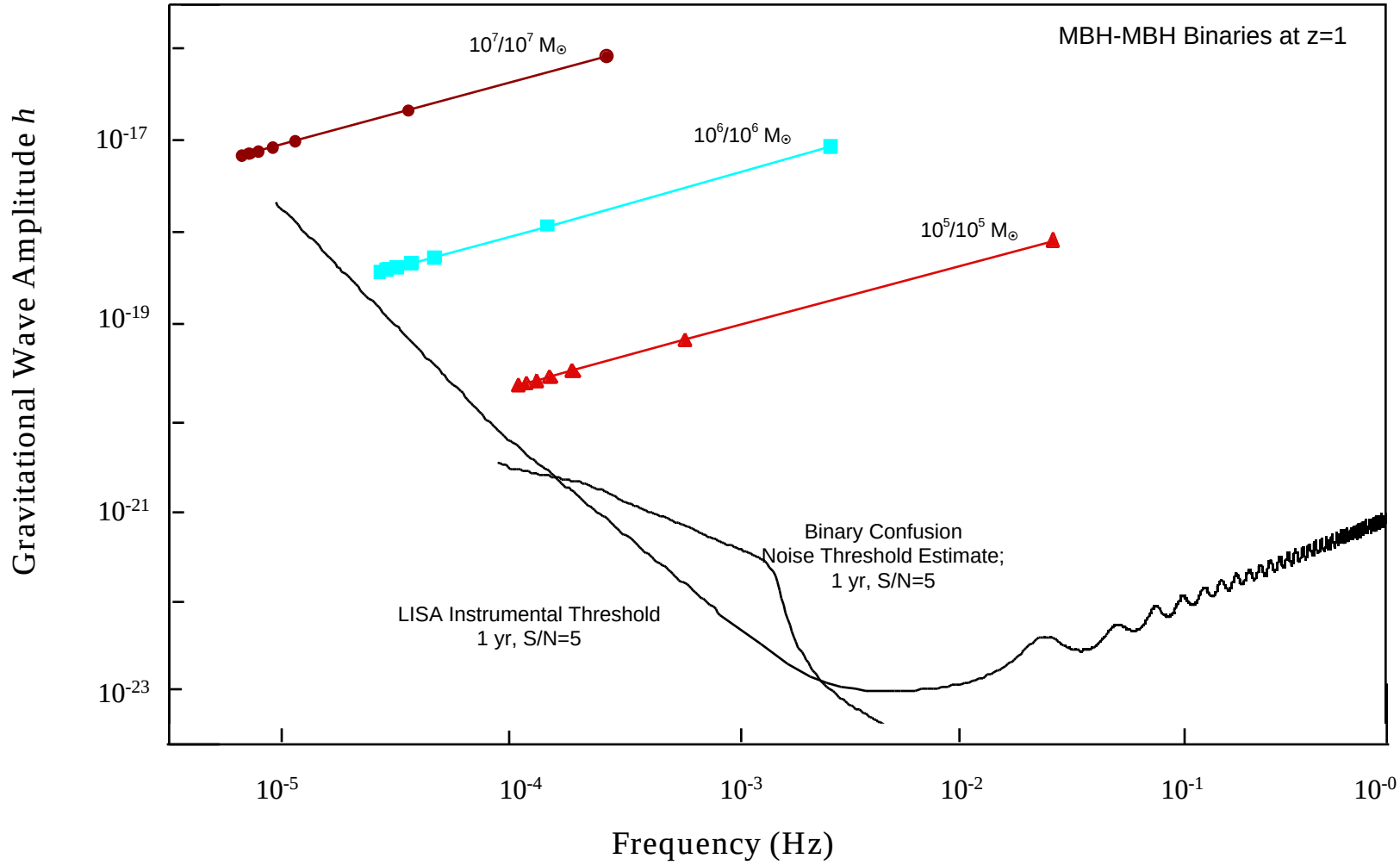

Mission Concept

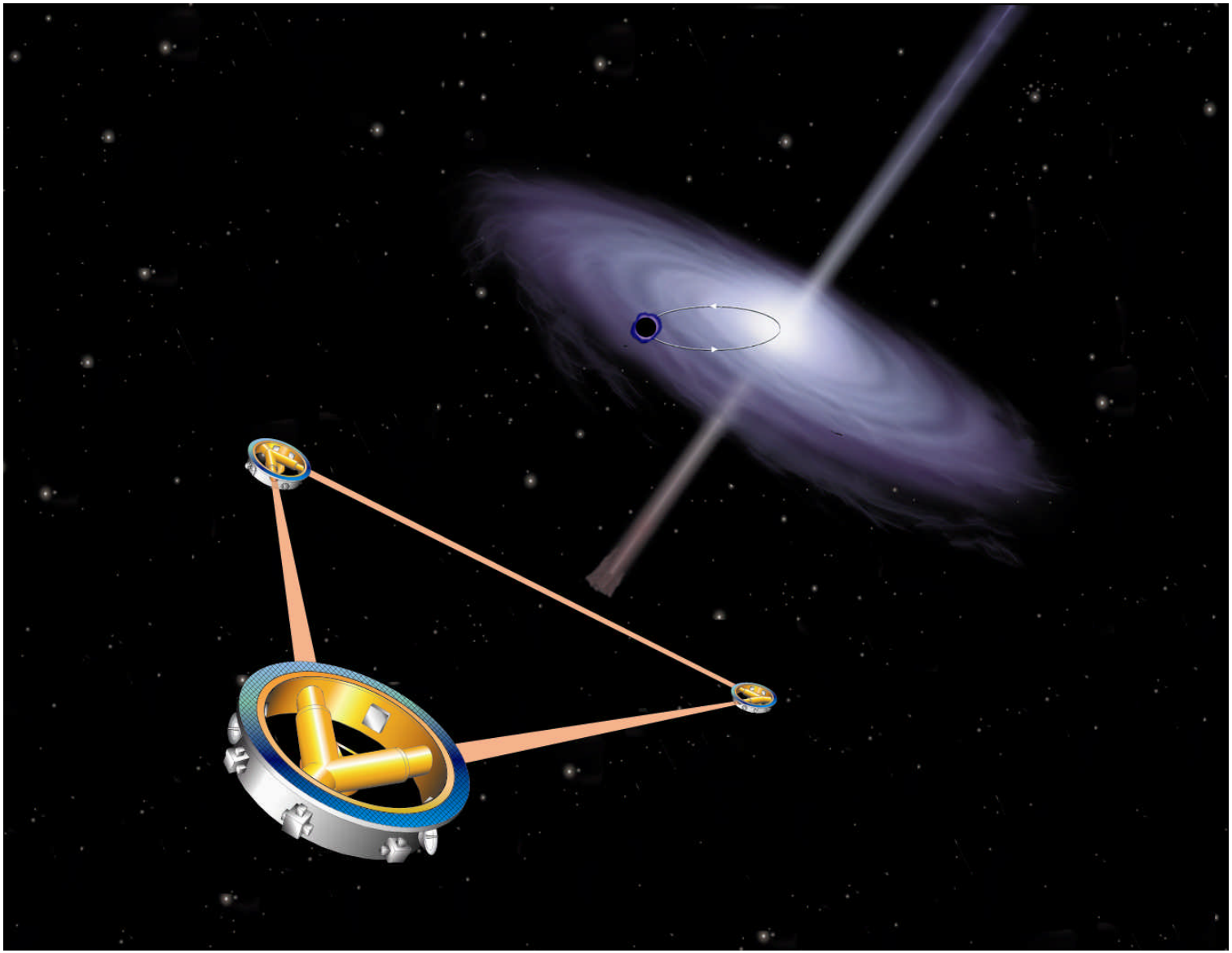

Spacecraft Orbits

- Spacecraft orbits evolve under gravitational forces only
- Spacecraft fly “drag-free” to shield proof masses from non-gravitational forces

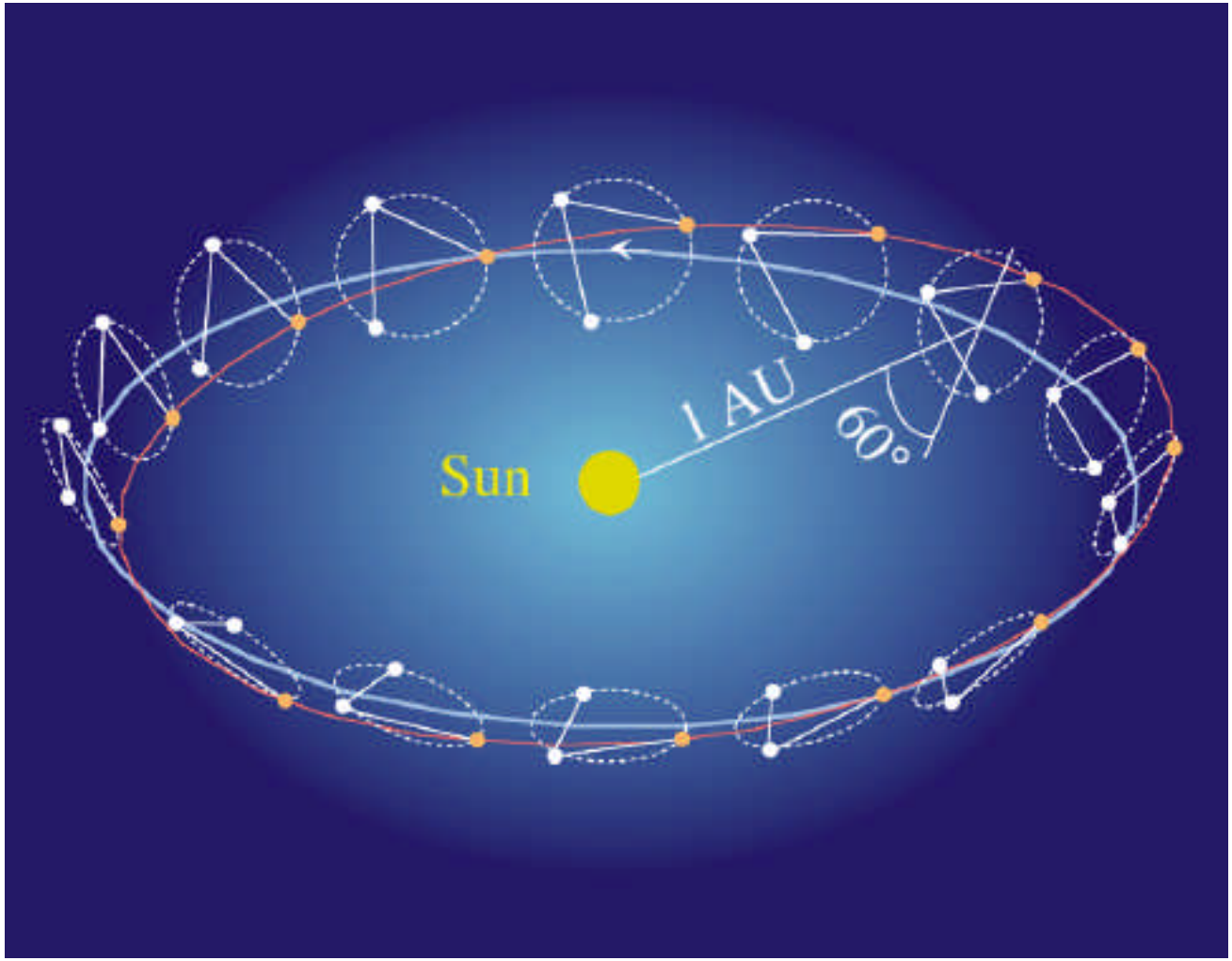

Optical System